NKS-502
ISBN 978-87-7893-600-4

Passive safety system performance of SMRs

Xicheng Wang[1]

Dmitry Grishchenko[1]

Pavel Kudinov[1]

[1]Division of Nuclear Science and Engineering

Royal Institute of Technology (KTH)

June 2025

Abstract

This work aims to develop and validate modeling approaches for key Passive Safety System (PSS) phenomena, and to establish reliability assessment methodologies. A major focus is steam condensation in water pools, commonly used as SMR heat sinks, where temperature distribution strongly influences natural circulation and passive heat removal. Due to limited predictive capabilities, the development of mechanistic model and large-scale experiments have been initiated, including several international projects. This report details analytical support for the OECD/NEA PANDA tests on steam injection into a water pool. Five tests were designed to address uncertainties in thermal stratification and mixing under pressurized, near-saturation conditions, using data-driven sensor placement for thermocouple positioning and combined Particle Image Velocimetry (PIV) to capture velocity and temperature profiles.

The report also reviews recent advances in PSS reliability analysis, emphasizing challenges in efficiently identifying Failure Domains (FDs).

Key words

Steam Condensation, Pool Stratification, Passive Safety System, Reliability Analysis, Small Modular Reactors

NKS-502
ISBN 978-87-7893-600-4
Electronic report, June 2025

NKS Secretariat
P.O. Box 49
DK - 4000 Roskilde, Denmark
Phone +45 4677 4041
www.nks.org
e-mail nks@nks.org

Development of the EHS/EMS models and modeling of PANDA and SEF-POOL experiments

Project: Passive safety system performance of SMRs (Contract: AFT/NKS-R(24)141/7)

Xicheng Wang, Dmitry Grishchenko, Pavel Kudinov

Royal Institute of Technology (KTH),
Division of Nuclear Science and Engineering
Roslagstullsbacken 21, 106 91 Stockholm, Sweden

2025
Stockholm

Table of contents

1. INTRODUCTION 4
1.1. Passive safety systems reliability of SMR *4*
1.2. Containment thermal-hydraulic phenomena *4*
1.3. Modeling of pool behaviors with steam injection *5*
1.4. Integral pool experiments in PANDA facility *7*
2. GOALS AND TASKS 9
3. PRE-TEST DESIGN OF PANDA P1A6 TEST SERIES 10
3.1. PANDA facility *10*
3.2. Numerical scheme *11*
3.2.1. EHS/EMS models 12
3.2.2. "Unit Cell" implementation 14
3.2.3. Boundary conditions 15
3.2.4. Turbulence model 16
3.3. Pre-test simulations in definition of injection procedures *17*
3.3.1. Interaction between LRR and SH injections 18
3.3.2. Injection procedures 20
3.4. Pre-test simulations in definition of instrumentations *21*
3.4.1. Sparse sensing and field reconstruction 22
3.4.2. Optimal sensor placement 24
3.4.3. Scoping simulations 24
3.4.4. Design of instrumentation 27
4. REVIEW OF METHODOLOGY FOR ANALYSIS OF PASSIVE SAFETY SYSTEM RELIABILITY 31
4.1. Importance of reliability analysis for PSS *31*
4.2. General steps for analysis of PSS reliability *32*
4.3. Summary of reviewed methodologies *34*
4.3.1. **REPAS:** Reliability Evaluation of Passive Safety Systems 34
4.3.2. **RMPS**: Reliability Methods for Passive Systems 35
4.3.3. **APSRA**: Assessment of Passive System Reliability 37
4.3.4. **ROAAM+**: Risk-Oriented Accident Analysis Methodology 39
4.4. Knowledge gaps and challenges *41*
ACKNOWLEDGEMENTS 43
DISCLAIMER 44
REFERENCES 45

EXECUTIVE SUMMARY

This report presents the progress of the project "Passive Safety System Performance of SMRs (PAS-SMR)", which aims to (i) develop and validate modeling approaches relevant to key physical phenomena associated with Passive Safety Systems (PSS), and (ii) develop methodologies for assessing the reliability of such systems. One of the critical phenomena affecting the performance of PSS in Small Modular Reactors (SMRs) is steam condensation in water pools, which frequently serve as the primary heat sink. The temperature distribution within these pools plays a significant role in the behavior of natural circulation, and consequently, in the effectiveness of passive heat removal. Due to limited predictive capabilities in this area, efforts have been initiated to develop mechanistic models and to conduct large-scale experimental campaigns. These include the OECD projects HYMERES, HYMERES-2, and the ongoing PANDA project (2021–2025).

This report details the analytical support provided for the design, pre-test analysis, and post-test validation of the OECD/NEA PANDA P1A6 test series involving steam condensation in a water pool. A total of five experiments have been designed, covering both injection procedures and instrumentation strategies, with the objective of addressing remaining uncertainties in thermal stratification and mixing under pressurized conditions, near-saturation states in the upper pool regions. A data-driven sparse optimal sensor placement strategy has been employed to determine Thermocouple (TC) locations, and a synthetic measurement, i.e. TCs together with a Particle Image Velocimetry (PIV), has been implemented to simultaneously capture downstream velocity and temperature profiles induced by steam injection. The experimental data generated will be used to validate and refine the developed mechanistic models.

In addition, this report presents a review of the most recent advancements in PSS reliability analysis. Based on this synthesis, a key challenge in the reliability analysis is the accurate and efficient identification of Failure Domain (FD) regions in the input space where the system fails to meet performance criteria. The next phase of the project will focus on developing a comprehensive approach for reliability assessment of PSS. This effort will leverage KTH's expertise in the analysis of natural circulation systems, including the study of flow instabilities, and the application of advanced search techniques such as genetic algorithms for identifying failure conditions in high-dimensional accident scenario spaces. The reliability framework will also incorporate comprehensive sensitivity and uncertainty analyses using the ROAAM+ methodology developed at KTH.

Keywords: Steam Condensation, Pool Stratification, Passive Safety System, Reliability Analysis, Small Modular Reactors.

1. INTRODUCTION

1.1. Passive safety systems reliability of SMR

Small modular rector (SMR) technology is a very likely candidate for new built in Europe including Nordic countries. Several designs of SMRs are currently at an advanced level of maturity, ready to be deployed. Passive safety systems (PSS) are widely used in all SMR designs and are viewed as the key to enhanced safety of SMRs.

PSS employs physical processes, such as natural circulation, instead of active elements (e.g. pumps and valves) that require external power to operate. Thus, the main challenge for assessment of passive systems reliability is that probabilistic safety assessment approaches that combine fault trees approaches to identify initiating events and event trees to calculate likelihood of failures are not directly applicable to analysis of passive systems. Instead, demonstration of passive system reliability requires mechanistic analysis of the system performance in all possible accident scenarios.

Accident scenarios along with design of the passive safety system define regimes and conditions for the physical phenomena that can lead to system malfunction. Heat removal is often the main goal of a passive system and the main driving force for its operation. At the beginning of a transient, heat is usually abundant and provides sufficient driving force for natural circulation. As the heat level drops with time, the driving force for the flow reduces, but still should be sufficient to remove the heat. Thus, reliability of a passive safety system must be demonstrated for a wide range of conditions, potentially including challenging oscillatory two-phase flows. Design of such systems, that can reliably work in a wide range of conditions, is a non-trivial task.

To facilitate licensing process of SMRs in Nordic countries it is important to demonstrate that:

- The mechanistic code used for thermal-hydraulic (TH) analysis has been adequately validated against experimental data relevant for the expected conditions and regimes of the passive safety system operation.
- The analysis of the system with the validated mechanistic code included all possible scenarios of the system operation (including non-trivial ones with different time delays for activation of different equipment and systems).
- The success criteria for operation of the passive system are clearly defined in terms of the system mission (this might include prevention of the reactor core damage, arrest of core degradation, prevention of vessel reactor failure after core degradation etc.).
- The “failure domains” i.e. the domains of scenario parameters where the passive system fails to fulfill its mission are clearly identified and respective “failure modes” of the system (physical mechanisms responsible for the failure are clearly understood).
- The approach for defining the likelihood of scenarios that lead to the failure of the passive safety system is coherent and complete.

1.2. Containment thermal-hydraulic phenomena

Containment is an essential part of the reactor safety design and is the last physical barrier that prevents the release of radioactive fission products into the environment. Large water pools are important elements of containment safety systems across various reactor designs. Large Light Water Reactors (LWRs) of Generation III+ are extensively using PSS and direct contact

condensation to suppress containment pressure in case of steam release from the primary system.

Many SMRs also incorporate PSS and water pools as ultimate heat sinks, facilitating passive decay heat removal during accident scenarios through natural circulation. For example, the Isolation Condensation System (ICS) in the BWRX-300 removes decay heat by condensing steam from the RPV into a heat exchanger (or condenser) submerged in a water pool located above the RPV. The pool also serves as a water source for several safety systems such as Emergency Core Cooling System (ECCS), spray, and as a scrubber in case of a core damage accident with release of radioactive aerosols.

Direct Contact Condensation (DCC) of steam into a water pool is a key phenomenon of the PSS of SMRs. Such pools are often served as the primary heat sink. Performance of the containment and its safety systems can be affected by interactions between (i) physical phenomena in the suppression pool, such as stratification and mixing induced by steam injection, and (ii) accident scenarios, such as failure/recovery of safety systems and timing of operation actions. A stratified pool will have higher temperature at the surface compared to a completely mixed pool with the same average temperature. The pool surface temperature determines the steam partial pressure in the containment gas space. Higher pool temperature results in higher partial pressure of steam in the containment atmosphere and respectively higher total containment pressure, while bottom layer of the pool remains cold. If the water temperature at the steam injection point is close to saturation, condensation can be very violent leading to large dynamic loads. If saturation conditions are reached in the vicinity of the steam injection, steam can bypass the pool without condensation. Thus, thermal stratification reduces pressure suppression capacity of the pool.

For instance, containment pressure in Fukushima Daiichi Unit 3 accident was rapidly increasing during the first 12 hours of the operation of the Reactor Core Isolation Cooling (RCIC) system [4, 5]. The system was driven by a steam turbine which exhaust is connected to the pressure suppression pool. The automated protection system shut down the RCIC when the pressure reached 400 kPa. The lumped parameter codes underestimated the rate of pressure increase and resulting maximum pressure by about 160 kPa using a mixed pool assumption [4]. The underprediction was attributed to the development of thermal stratification in the suppression pool.

The evolution of thermal behavior of the pool depends on the assumption about the fraction of the pool volume that can be considered as a heat sink, which is treated with necessary conservatism. However, there are no higher fidelity tools available to confirm that the current assumption is indeed conservative. Furthermore, the conservative approach cannot provide adequate predictions of pool temperature transient, i.e. elevation of the thermocline as a function of time. Analyses of realistic accident scenarios that can adequately resolve the interplay between phenomena, safety systems, and operational procedures require the development of more mechanistic models that do not rely on conservative assumptions. The results of such models should also provide an opportunity to verify conservatism in the safety analysis.

1.3. Modeling of pool behaviors with steam injection

The prediction of pool behaviors remains a challenging task, because of the (i) lack of adequate mechanistic models suitable for system analysis codes to capture transient 3D phenomena in

the pool and (ii) unaffordable computational costs for predicting DCC phenomena [6, 7, 8] using Computational Fluid Dynamics (CFD) codes with explicit resolution of the interface between steam and water, especially for long term transients in large-scale pools.

To address this challenge, Effective Heat Source (EHS) and Effective Momentum Source (EMS) models [1, 2, 9] have been proposed to enable the prediction of thermal stratification and mixing phenomena in a BWR containment and pressure suppression pool (Figure 1). The EHS/EMS models have been under development for steam injection through the blowdown pipes [1, 2, 9, 10, 11, 12, 13, 14, 15, 16, 17, 18, 19, 20, 21, 22] and the spargers [23, 24, 25, 26, 27, 28, 29, 30, 44]. The models provide a computationally efficient method by exploiting the gap between the spatial and temporal scales of the large pool and direct contact condensation phenomena. The models postulate that the effects of steam injection on the development of thermal stratification and mixing in a large pool can be predicted using only "effective" (time-averaged) sources of heat and momentum created by steam injection without explicit resolution of the steam-water interfaces.

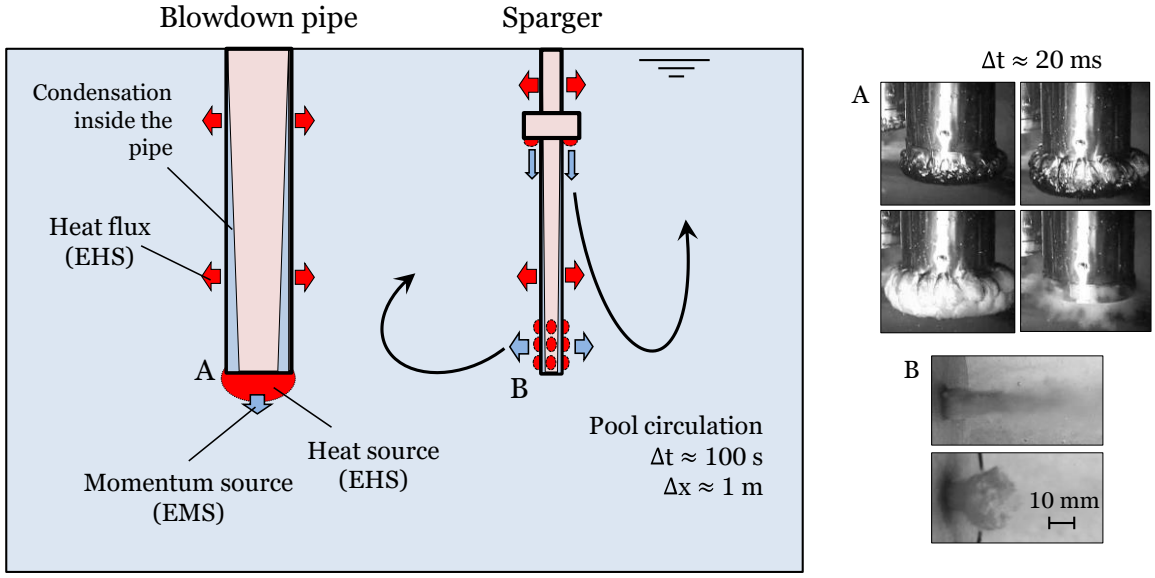

Figure 1: Illustration of EHS/EMS distributions induced by steam injection through blowdown pipes and multi-hole spargers. Image (A) refers to PPOOLEX PAR-11 experiments [33] and (B) SEF-POOL experiments [35].

To obtain experimental data necessary for model development and validation, fruitful cooperation has been established with experimental teams at Lappeenranta University of Technology (LUT) in the framework of NKS and NORTHNET RM3 projects and Paul Scherer Institute (PSI) in the framework of the OECD/NEA HYMERES and HYMERES-2 projects. Researchers at KTH carried out pre-test analysis for development of the experimental design and test matrixes for PPOOLEX and SEF-POOL tests at LUT and PANDA tests at PSI, and post-test validation of the models against available experimental data from these tests [31].

EHS/EMS models for spargers were originally developed using the data from respective PPOOLEX and PANDA tests. These models were applied to analysis of a prototypic plant scale model of the pressure suppression pool [34]. Results of the analysis suggested that strong stratification in the pool can develop depending on the conditions of steam injection through different number of spargers. The case where all steam condensed inside the pipe (3.5 kg/s through 64 spargers) led to a non-uniform heat distribution in the hot layer, reaching 95 ℃ pool surface temperatures 7.7 h after the beginning of the blowdown. At larger steam mass flows

(9.0 kg/s through 64 spargers) some fraction of steam was injected through the LRRs. This led to a stronger mixing and more uniform temperature distribution in the hot layer. Nevertheless, the pool surface temperature reached 95°C after 6.7 h of transient.

Plant analysis was also recently carried out with the latest versions of the EHS/EMS models (details of the model development can be found in [41, 42, 44]) in the framework of the SSM-PSP project. Results also indicate that development of pool stratification is quite possible [46] if momentum source is relatively weak (even in case of relatively large steam flow rates when steam is supplied through a large number of spargers). To achieve pool mixing, activation of the high momentum nozzles is often necessary, and requires considerable amount of time.

Although significant progress has been made in model development and there is indication that thermal stratification is likely to develop in case of steam injection through spargers in a prototypic scale pool, there are several aspects, which require further work to apply EHS/EMS models more reliably to analysis of realistically complex plant scenarios.

Previous work on the EHS/EMS models validation confirmed that predictive capabilities can be developed for simulation of fast mixing and slow erosion of the stratified layer, observed in the PPOOLEX and PANDA experiments with steam injection through spargers and blowdown pipes. The Separate Effect Facility (SEF-POOL) was constructed at LUT with the help from KTH in the design process. The purpose of the facility was to provide a direct measurement of the effective momentum. In the SEF tests steam is injected into the pool through the sparger pipe [35, 45].

The combination of the integral and separate effect data was used to further develop and validate the EHS/EMS models [44]. One of the main remaining sources of uncertainty in modeling is the modeling of the turbulence characteristics induced by steam injection. New experimental data are needed to reduce the modeling uncertainty.

1.4. Integral pool experiments in PANDA facility

After the Fukushima Daiichi, BWRs research community realized that some of the containment phenomena that have a significant impact on the accident progression could not be reliably predicted by contemporary safety analysis tools. This realization reignited the international research community with an interest in containment and pool behavior. OECD/NEA HYMERES-1 project (2013-2016) was the first internationally supported effort that addressed pressure suppression pool phenomena in a dedicated HP5 series of experiments in PANDA facility which is a unique, large-scale, multi-purpose facility well instrumented for performing thermal-hydraulics experiments on containment phenomena. A schematic for the PANDA test configuration addressing the suppression pool is shown in Figure 2. The tests involve the interplay of different compartments e.g. Drywell, Wetwell, RPV and components e.g. venting pipes, vacuum breaker, spray, etc.

In the HP5 series [32], experiments were conducted in two sequential phases to investigate thermal-stratification build-up and subsequent homogenization in a water pool at various initial temperatures. Steam was introduced through a vertical sparger and, in separate tests, water was injected via a horizontal nozzle. By varying the steam flow rate, the tests demonstrated that low flow rates promoted thermal stratification, whereas high flow rates resulted in rapid thermal homogenization. In one test, a mixture of helium/steam was vented in phase 2 and the homogenization time was drastically reduced. Also, for the tests in which water was injected

through a horizontal nozzle in phase 2, the water temperature was varied in different tests to enhance either buoyancy or inertia of the water jet.

Building on the success of HYMERES-1, the OECD/NEA HYMERES-2 project (2017–2021) was launched to address remaining uncertainties in suppression-pool and BWR system behavior. A primary aim of HYMERES-2 is to quantify the rate of thermocline erosion as a function of (i) the distance between the steam-injection point and the thermocline and (ii) the steam injection direction—radial through the sparger head versus downward through the load reduction ring [43].

Right after HYEMERES-2, OECD/NEA is launching the third phase of the project called PANDA-1 (2021-2025), aiming to perform experiments in PANDA facility to address complex safety issues for current water reactors and SMRs. Several topics proposed in the PANDA tests are of direct relevance to containment thermal-hydraulic phenomena:

- Topic 1: Extend the database at large scale on flow interacting with containment internal structures and on thermal radiation (P1A1 and P1A2 series).
- Topic 2: Extend the database on activation of PWR containment spray system (P1A3 series)

- Topic 3: Small Modular Reactor (SMR) system tests (P1A4 and P1A5 series).
- Topic 4: Extend the database on pressure suspension pool of BWRs and IRWST of PWR (P1A6 series)

New experimental data that will be obtained in OECD/PANDA project will be very helpful to reduce the uncertainty in the modeling.

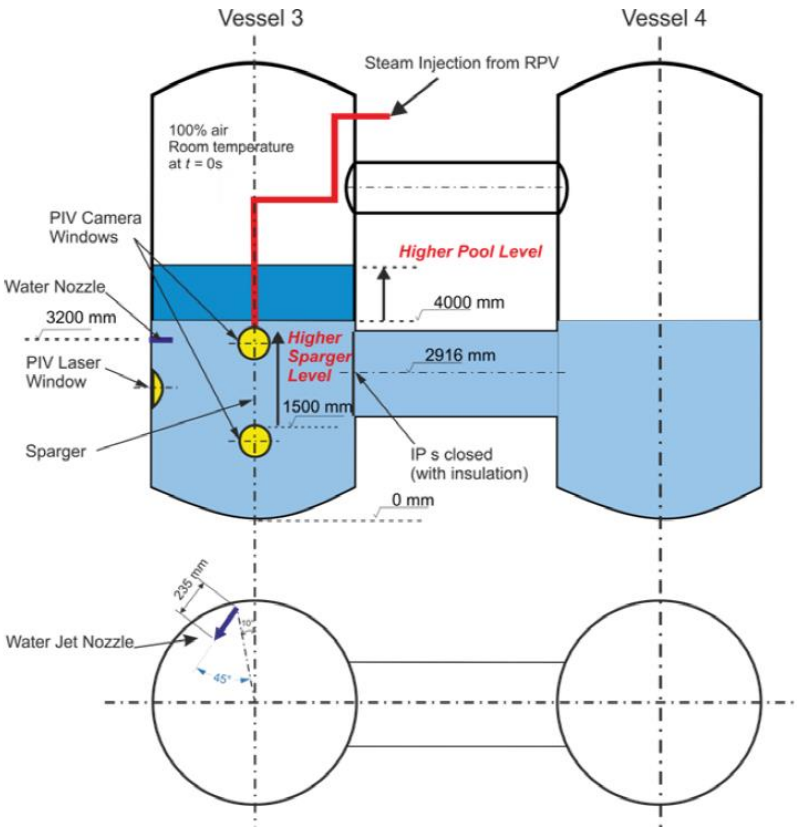

Figure 2: Example for the PANDA test configuration addressing suppression pool

2. GOALS AND TASKS

The goal of the project will focus on (i) development and validation of modeling approaches relevant to important phenomenology of passive safety systems, (ii) development of approaches to assessment of passive safety system reliability. One of the important phenomena relevant to SMR passive safety systems is steam condensation in a pool of water. Such pools are often used the main heat sink. Temperature distribution in the pool can significantly affect performance of natural circulation passive safety systems. The lack of predictive capabilities has led to the initiation of (i) development of mechanistic models, and (ii) experimental campaigns including a series of OECD projects HYMERES, HYMERES-2 and currently ongoing (2021-2025) PANDA project.

KTH is a recognized leader in both model development and analytical support for the design and interpretation of the large-scale tests in the OECD projects Development of the Effective Heat Source (EHS) and Effective Momentum Source (EMS) models was initiated at KTH to enable mechanistic modeling of the pool transients. Experimental data from previous PANDA tests designed by KTH were very instrumental for model development and validation.

In this work, KTH will provide analytical support to the design, pre-test analysis and post-test code validation against OECD/NEA PANDA project tests series P1A6 with steam condensation in the pool. Obtained data will be used for validation and further improvement of the developed models. KTH will work on development of approaches to assessment of passive safety system reliability. The approach will build on experience of KTH in analysis of natural circulation systems including instabilities, use of advanced search methods such as genetic algorithm to identification of “failure” conditions in the multidimensional space of accident scenario parameters, comprehensive sensitivity and uncertainty analysis using developed at KTH ROAAM+ approach.

In 2024, the following main tasks to be addressed to achieve the goal of the project:

- Task1: KTH will focus on pre-test analysis and post-test validation against OECD/PANDA test series P1A6. The target of the tests will be clarification of remaining uncertainties in the stratification and mixing of the pool at higher pressure condition, including near-saturation conditions in the upper part of the pool.
- Task2: KTH will review most recent developments in the area on passive system reliability analysis. Based on the synthesis of the review the knowledge gaps will be identified for further improvement of the methods, specifically applicable to systems such as BWRX-300.

3. PRE-TEST DESIGN OF PANDA P1A6 TEST SERIES

This section presents the pre-test analysis conducted to support the design of the P1A6 test series within the framework of the OECD/PANDA project. The series comprises several tests designed to investigate thermal behaviors in the suppression pool induced by steam injection through a sparger. The safety relevant thermal-hydraulic phenomena are the development of thermal stratification and erosion of the thermocline.

The main goals and objectives of the P1A6 test series are as follows:

- To conduct the first test series investigating the interaction between the steam injection through Load Reduction Ring (LRR) and multi-hole Sparger Head (SH).
- To study the erosion of a strong thermocline, including conditions with high steam flow rates up to 400 g/s.
- To assess the effects of pool pressurization.
- To explore condensation regimes under low Jakob number (i.e., low subcooling) conditions, including regimes such as incomplete condensation that have not been assessed in previous tests.
- To represent plant-relevant scenarios, particularly those involving steam injection that begin at high flow rates and gradually decreases.
- To provide high-resolution data on both global and local pool phenomena for model development and code validation.

The parameters required to be determined through pre-test analysis are (i) elevation of sparger tip above pool bottom, (ii) flow rate and duration in each injection phase, and (iii) configuration of instrumentation, e.g., Particle Image Velocimetry (PIV), Thermocouples (TCs).

The remaining content in this section are structed as: Section 3.1 review the specifications of the PANDA facility employed in previous sparger experiments, Section 3.2 details the numerical setup for the pre-test simulations, Section 3.3 discusses the results of pre-test simulations in definition of the experimental matrix and Section 3.4 presents the pre-test analysis in support of the instrumentation design.

3.1. PANDA facility

PANDA [38] is a multipurpose test facility designed to address containment thermal-hydraulics phenomena and safety issues in Light Water Reactors (LWRs). The facility contains 2 drywells, 2 wetwells, 1 Gravity Driven Cooling System (GDCS) tank, and an RPV vessel with a steam generator of 1.5 MW. All the sparger experiments were performed in one of the wetwell vessels as exampled in Figure 3.

The geometrical specifications of the sparger placed along the central axis of the pool is illustrated in Figure 4. The multi-hole Sparger Head (SH) contains 32 holes arranged in 4 rings to inject steam radially outwards, and the Load Reduction Ring (LRR) contains 8 holes in 1 ring to inject steam vertically downward. LRR is designed in the plant to reduce dynamic loads on the sparger pipe, and it is located at $1.8\ m$ above the SH. Each hole has an inner diameter of $9.5\ mm$ and a conical chamfer. The hole at the tip of the sparger was blocked during the test.

The safety relevant phenomena studied in this work are the development of thermal stratification and the dependence of the erosion rate of thermocline on the steam injection and pool conditions. The regimes that are expected during most of the anticipated scenarios are sub-sonic condensation regimes where the maximum steam flux can reach ~200 kg/(m^{2}s).

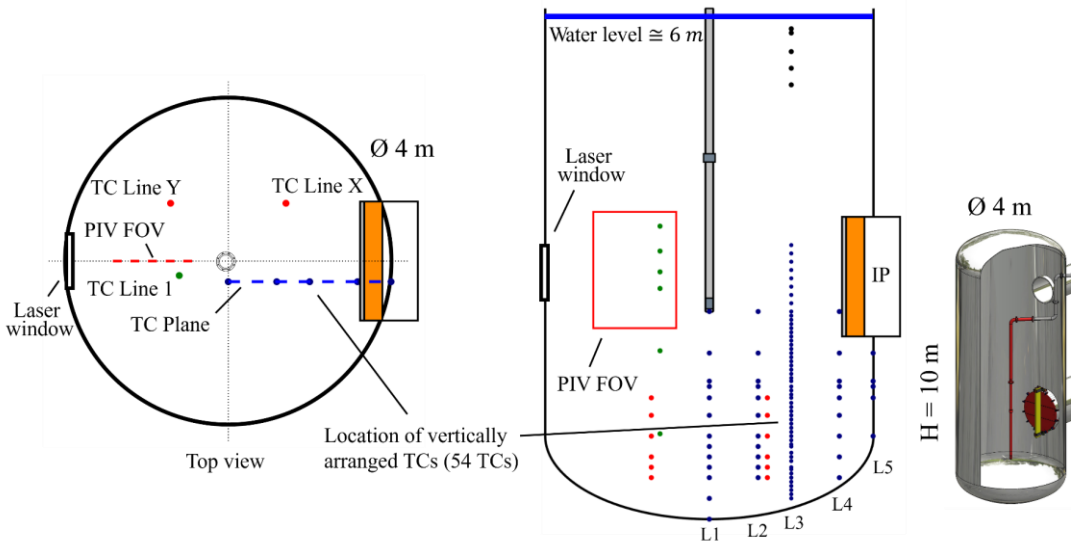

Figure 3: Instrumentations of sparger tests performed in PANDA facility during previous HYEMRES-2 project [47].

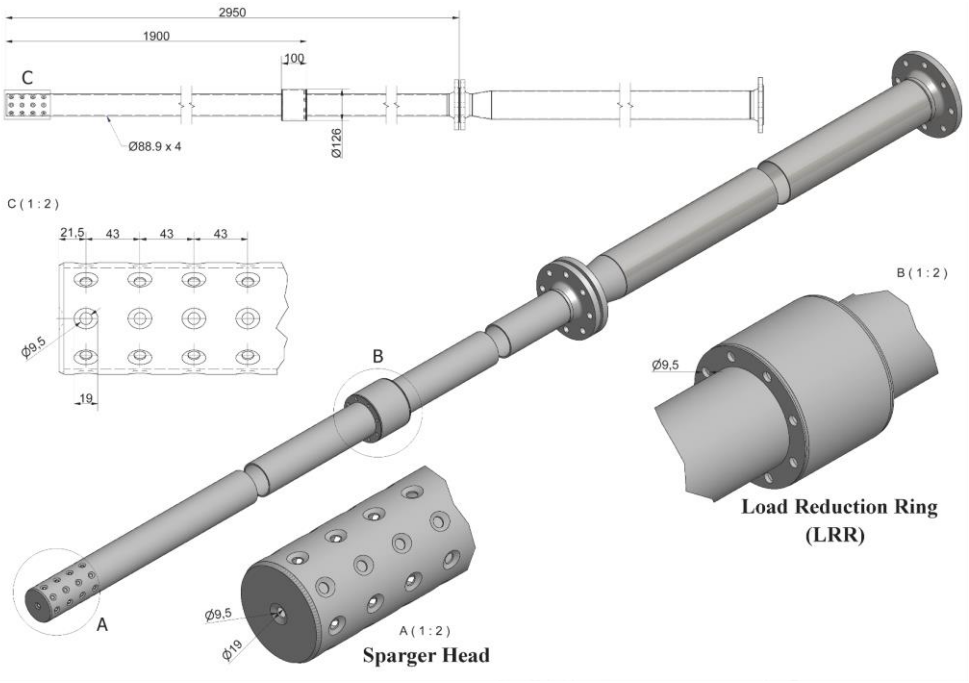

Figure 4. Geometry of the sparger pipe in PANDA tests.

3.2. Numerical scheme

The pre-test analysis was performed by CFD simulations with EHS/EMS models implemented in ANSYS Fluent 2021 R2 [39] using a single-phase solver. Water properties were determined by piecewise polynomial profiles as functions of temperature. Energy equation was turned on to include the effect of buoyancy and the dynamic mesh was used to enable the motion of the

pool surface to accommodate increasing water pool level. All simulations were considered fully converged with the residual below 1e-6 for energy and 1e-4 for the other variables.

3.2.1. EHS/EMS models

Direct Contact Condensation (DCC) of steam injected into a water pool is as a source of heat and momentum. A competition between these sources determines whether the PSP will be thermally stratified or mixed [1, 2]. Momentum depends on the steam condensation regime e.g. chugging, oscillatory bubbles, and stable jets. If steam injection results in a low momentum source incapable to overcome buoyancy forces, the heat can be deposited in the layer above the injection point, while water below remains cold [3]. If steam injection results in a higher momentum source, leading to the development of a large-scale circulation in the pool which can erode or even break the stratification [3].

Explicit modeling of direct contact condensation of steam is a challenge for contemporary codes. The small time and length scale of steam condensation behavior requires very small mesh size and time step when using CFD type analysis [6, 7, 8]. Lumped and 1D codes are inadequate for prediction of 3D, transient mixing phenomena. Thermal-hydraulic codes such as GOTHIC [36], and RELAP5 [37], do not provide a model for prediction of the effect of steam injection through blowdown pipes or spargers. Available condensation models are mostly designed for pipe flow regimes such as bubbly, churn, film, etc.

Therefore, the concept of Effective Heat Source (EHS) and Effective Momentum Source (EMS) models have been proposed to enable the prediction of the pool behavior induced by the steam condensation. The main idea of the effective models is that large scale pool behavior is not affected by the details of the DCC phenomena occurring at the small temporal and spatial scales. Therefore, only the time-averaged "effective" heat and momentum sources induced by steam in a large pool need to be modelled. The effective heat Q_{eff} and momentum M_{eff} sources can be presented as [2]

$$Q_{eff}(t) = \frac{1}{\Delta t} \int_{t-\Delta t}^{t} Q(\tau) d\tau \quad (1)$$

$$M_{eff}(t) = \frac{1}{\Delta t} \int_{t-\Delta t}^{t} M(\tau) d\tau \quad (2)$$

where the integrals represent the time-average of the instantaneous variations of the sources over a period Δt of time. These variations are due to the oscillatory nature of direct contact condensation. For example, the large-scale motions of the liquid inside the pipe during the chugging regime, the small-scale oscillatory bubble behavior, etc.

The chart for estimation of the effective heat and momentum sources in the EHS/EMS models is shown in Figure 5. First, condensation regime is estimated for the given steam injection and pool conditions, then respective heat and momentum sources are calculated.

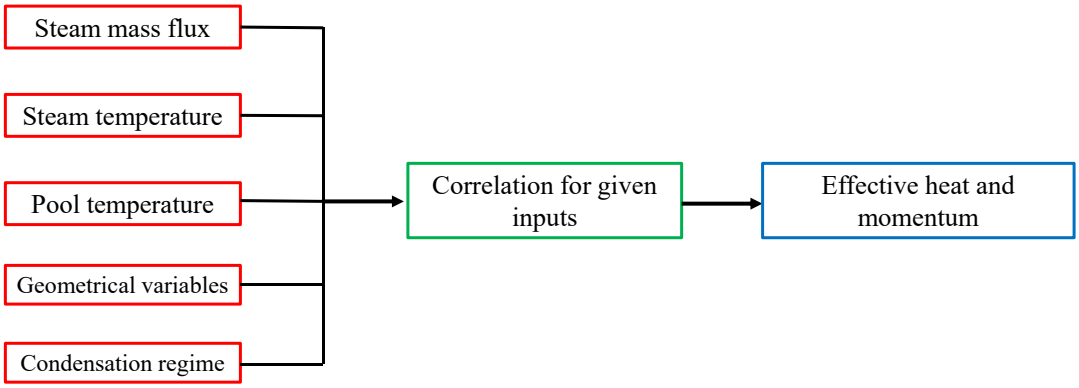

Figure 5. Chart of the EHS/EMS models.

The effective momentum source used in this work is introduced as:

$$M_{eff} = CM_{th} = C\left(\rho_s A_i U_s^2 + A_i(P_s - P_\infty)\right) \tag{3}$$

where M_{th} is the theoretical momentum rate; ρ_s and P_s the steam density and pressure at the injection holes; P_∞ the hydrostatic pressure of the pool; U_s the steam velocity; A_i the total injection hole area; C is a non-dimensional coefficient that takes into account the effect of the condensation regimes on the momentum rate transferred to the downstream liquid flow.

The magnitude of the condensation coefficient C was first measured in the SEF-POOL facility, where steam was injected through a single or multiple holes into a subcooled pool with constant mass fluxes [35]. Experimental measurements show that C is strongly dependent on the Jakob number in the sub-sonic regimes and remains nearly constant in the sonic regime. The empirical correlation was further improved by involving the effects of Mach number and pitch-to-diameter (P/D) ratio as shown in Figure 6 and it reads:

$$C = \frac{C_1\phi_1 + C_2\phi_2 + C_3\phi_3 + C_4\phi_4}{\phi_1 + \phi_2 + \phi_3 + \phi_4} \tag{4}$$

where $C_1 \sim C_4$ are closure coefficients and $\phi_1 \sim \phi_4$ are blending functions. The detailed formulations of each term are detailed in [45].

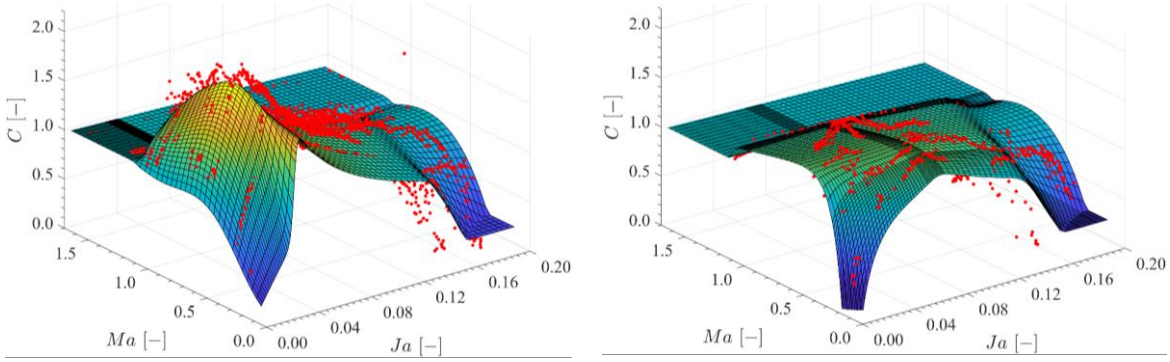

(a) (b)

Figure 6. Illustration of fitted surface for (a) $P/D = \infty$ and (b) $P/D = 2, 3.25, 4.5$ using measurements (i.e. red points) from SEF-POOL experiments [45]. (b) is an improved version compared to the one in [45] to enable a better fitting and a smoother transition among regions.

For the effective heat induced by all condensation regimes, it can be determined by the enthalpy balance as:

$$Q_{eff} = \dot{m}_s h_s \tag{5}$$

where $\dot{m}_s$ and h_s are the mass flow rate and enthalpy of the steam.

3.2.2. "Unit Cell" implementation

Thermal stratification and mixing in a large pool are determined by a competition between buoyancy and momentum induced by the injected steam. Velocity of the jet in the downstream of steam condensation region develops a self-similarity profile similar to the single-phase turbulent jet [47]. Modeling of individual jets induced by steam injection through multi-hole SH and LRR holes can be achieved by using single-phase liquid with the effective momentum and heat estimated by Eqs. (1)~(5).

This approach is called "Unit Cell" implementation and is illustrated in Figure 7a. EHS/EMS models were introduced by imposing boundary conditions (see Section 3.2.3) at the sparger surface. By doing this, the interaction among the individual jets from multi-hole SH as well as the interaction between the LRR jets and merged SH jets can be resolved to provide a better understanding of the local phenomena in the vicinity of the sparger.

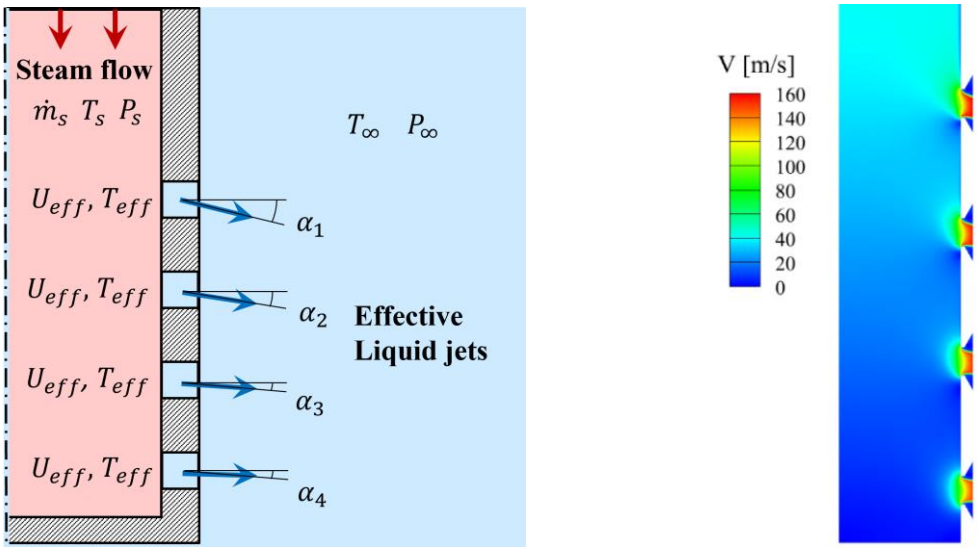

(a) (b)

Figure 7. (a) Schematic of "Unit Cell" implementation for SH and (b) velocity contours obtained by internal flow simulation of PANDA sparger using steam with $\dot{G}_s = 71\ kg/m^2 s$ [44].

The computational domain for the PANDA pool with "Unit Cell" implementation is presented in Figure 8. The height of the water level and sparger tip are 4 m and 3.7 m above the bottom of the pool. Previous study [41, 42] suggests that a $1/16$ sector domain (22.5°) is insufficient to resolve the flow pattern in the pool. Both 180° and 360° domains can provide reasonable results for temperature evolution. Thus, we use the 180° domain in this work to improve computational efficiency.

The pool mesh was created with polyhedral cells on the surface and hexahedral cells inside the fluid region (poly-hexacore meshing in ANSYS [39]). Smooth transition from the sparger tip to the surrounding wall was applied and the mesh below the sparger tip was refined in order to better capture the evolution of thermocline. Mesh sensitivity study of similar geometry can refer to this work [27].

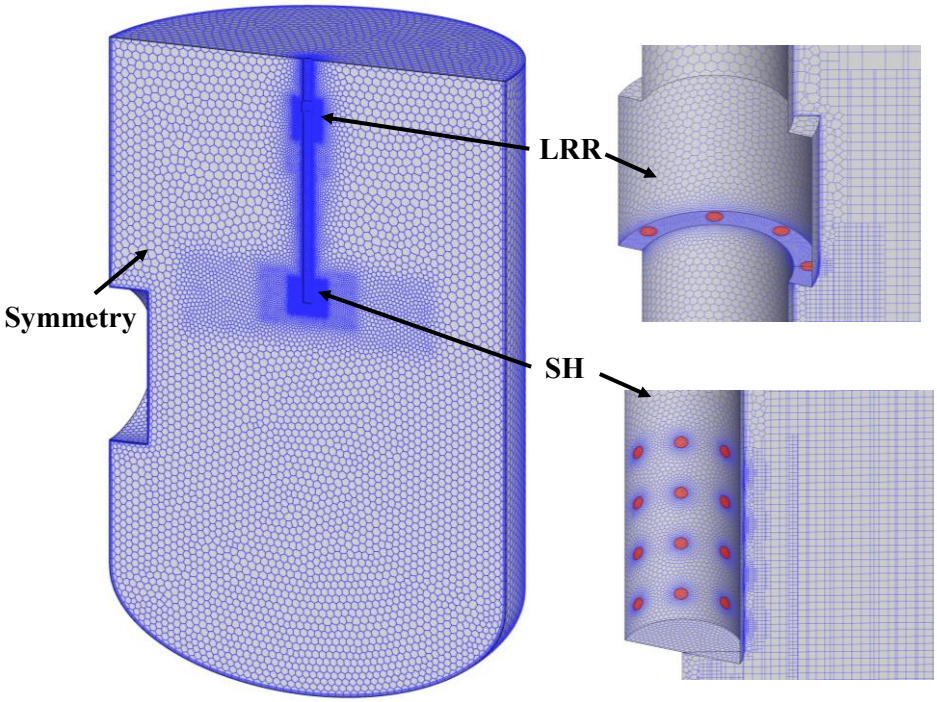

Figure 8. Computation domain of PANDA pool.

3.2.3. Boundary conditions

For jets discharged from LRR holes, the steam flow rate was assumed evenly distributed and normal to the inlet surface. While for the SH injection, the distribution of the steam flow and its downward angles among different elevations were determined by an internal flow simulation (Figure 7b). The simulation results [44] suggest the variation of these angles toward different steam fluxes (70~160 kg/m^2s) varies little, providing averaged angles of $14°, 12°, 9.5°, 0°$ from up to down. Similarly, the difference in steam flow rates among different holes is within $\pm 2.0\%$ and a uniform distribution was assumed. The flow distribution between LRR and SH holes is obtained from internal flow simulations and summarized in Table 1.

Table 1. Steam distribution through PANDA sparger with different flow rates.

Flow rates [g/s]	**LRR**		**Sparger head**	
	Steam flow $\dot{m}_{LRR}$ [g/s]	Steam flux $\dot{G}_{LRR}$ [kg/(m^{2}s)]	Steam flow $\dot{m}_{SH}$ [g/s]	Steam flux $\dot{G}_{SH}$ [kg/(m^{2}s)]
160	62.1	109.6	97.9	43.1
260	72.1	125.1	187.9	82.9
360	85.1	150.2	274.9	121.2
450	100.7	177.6	349.3	154.0

As shown in Figure 7a, effective liquid jets were introduced by imposing uniformly distributed velocity and temperature profiles on each injection hole. The effective momentum rate by Eq. (3) can be formulated by effective liquid velocity as:

$$M_{eff} = C\left(\rho_s A_i U_s^2 + A_i(P_s - P_\infty)\right) = \rho_l A_i U_{eff}^2 \tag{6}$$

In sub-sonic regimes where P_s is assumed to equal to P_∞, the effective velocity is written as:

$$U_{eff} = \sqrt{\frac{C\rho_s}{\rho_l}} U_s \tag{7}$$

where ρ_l is the liquid density, C the condensation regime coefficient calculated by Eq. (4).

Since the momentum created by steam was modeled by water injection, the respective mass flow rate of water was higher than that of steam injection. To preserve the mass balance, a fraction of injected water should be taken out from the pool with a total mass flow rate given by Eq. (8).

$$\dot{m}_{out} = \dot{m}_{in} - \dot{m}_s \tag{8}$$

where $\dot{m}_{in}$ is the total mass flow rate of the effective liquid and $\dot{m}_s$ the mass flow rate of steam. the water that should be removed $\dot{m}_{out}$ applied on the pool surface.

Heat balance was achieved by the time-averaged heat source provided by the EHS model given by Eq. (5). In these cases, when mass was taken out from the pool, the energy would be removed too. Therefore, to preserve the heat balance, the enthalpy of the injection water h_l^{in} should be defined that:

$$\dot{q}_{in} = \dot{q}_s + \dot{q}_{out} \tag{9}$$

$$h_l^{in} \cdot \dot{m}_{in} = h_s \cdot \dot{m}_s + h_l^{out} \cdot \dot{m}_{out} \tag{10}$$

The h_l^{in} is implemented by setting the temperature on inlet boundary according to Eq. (11).

$$T^{in} = \frac{h_l^{in}}{C_p} \tag{11}$$

where sub-indexes l and s are indicating liquid and steam respectively, in and out are indicating the input and output, C_p and T are the specific heat capacity and water temperature, respectively.

3.2.4. Turbulence model

Stable stratification with a significant temperature difference between the cold and hot layers was observed in all PPOOLEX and PANDA experiments. The development of the stratified layer is governed by buoyancy, which is modelled by the temperature-dependent water density. To model the effect of buoyancy on turbulence, source terms for turbulent kinetic energy k and

specific dissipation rate ω were modified respectively. Details of the turbulence model implementation can be found in [27].

The turbulence model was $k-\omega$ BSL model with low-Re corrections which provided the best agreement between prediction and experimental temperature evolution in PANDA & PPOOLEX pool tests [27]. Kato-Launder production term and production limiter are turned on to limit the build-up of k in the stagnation regions (i.e. the cold layer below the thermocline).

Extremely high turbulent intensity was observed in PIV measurement in PANDA tests [32] with steam injection in the oscillatory bubble regime. Measurement in SEF tests [47] suggests that with the same amount of effective momentum, the jet induced by steam injection diffuse much more than the liquid injection. Previous validation against PANDA and PPOOLEX pool tests showed that a good agreement on temperature evolution can be achieved if a high-level turbulence (e.g., turbulence intensity I=70%, and turbulent viscosity ratio μ_t/μ_l = 3000) is introduced at the inlet boundaries [41, 42].

However, this high-level turbulence introduced by setting large I and μ_t/μ_l on inlet boundaries dissipated rapidly by using RANS turbulence models as those models were calibrated against single phase turbulence flow. In reality, turbulence is not generated at the inlet but in the downstream region where the interface of condensing steam creates rapid motion of the ambient liquid. Therefore, an extra source term S_k that represents the effect of condensation induced turbulence is introduced in the transport equation of k and it can be written as:

$$S_k = \begin{cases} \frac{3}{2}\left(v_m I_{eff}\right)^2 \rho_l \frac{1}{\tau}, & v_m \geq U_{eff} C_{limit} \\ 0, & v_m < U_{eff} C_{limit} \end{cases} \quad (12)$$

where v_m and U_{eff} are cell velocity and effective velocity; I_{eff} is introduced to relate the generation of turbulence to local average velocity v_m and is called an "effective turbulent intensity"; τ is a characteristic time scale (assumed to be unity), ρ_l is liquid density. C_{limit} is a global filter based on the local averaged velocity that determines the region where S_k should be imposed (assuming that turbulence is actively generated in the region where local velocity is larger than $U_{eff}C_{limit}$). In this work, $I_{eff} = 2.5$ and $C_{limit} = 0.1$ were applied. Model validation and parameters analysis can be found in [44].

3.3. Pre-test simulations in definition of injection procedures

The test planned in PANDA project aims to investigate the thermal stratification induced by steam injection through the sparger. The goal is to obtain data on how the development and erosion of the thermocline are affected by (i) activation of both SH and LRR holes (ii) the high temperature gradient across the thermocline. CFD simulations conducted for pre-test analysis are summarized in Table 2 and the results are used to determine the test conditions of (i) elevation of sparger tip above pool bottom, (ii) flow rate and duration in each injection phase, and (iii) configuration of instrumentation.

Simulation with a sparger placed 2.5 m above the pool and opening of both LRR and SH holes suggests that the thermocline might be completely eroded at the end of the injection phase with $\dot{m}_s = 450 g/s$. Meanwhile, a larger submergence also requires a longer injection time to

achieve a strong stratification. Therefore, the sparger was lifted from 2.5 m to 3.7 m, leaving 0.5 m between LRR holes and the pool surface. All simulations were running with a 6 m water level and 15 ℃ initial pool temperature.

Table 2. List of simulations carried out for first series of pre-test analysis.

Case	Holes opened?		Phase 1		Phase 2		Phase 3		Phase 4	
	SH	LRR	Flow rate[1]	Duration	Flow rate	Duration	Flow rate	Duration	Flow rate	Duration
	-	-	g/s	s	g/s	s	g/s	s	g/s	s
C1	Yes	No	97.9	6000	187.9	4000	274.9	4000	349.3	4000
C2	No	Yes	62.1	6000	72.1	4000	85.1	4000	100.7	4000
C3	Yes	Yes	160	6000	260	4000	360	4000	450	4000
C4	Yes	Yes	160	12000	260	6000	360	3000	450	3000
C5	Yes	Yes	160	18000	260	6000	360	4000	450	4000

[1] Total steam flow rate through the pipe. The distribution between LRR and SH holes can refer to Table 1.

3.3.1. Interaction between LRR and SH injections

The interaction between LRR and SH injections was studied in Cases C1~C3 in which LRR and SH holes were opened individually and then opened together (Table 2). The steam flow rates in C1 and C2 were set to ensure the injected steam creates the identical amount of momentum source at LRR or SH holes compared to C3 (Table 1).

The snapshots of temperature fields among these three cases obtained at end of second injection phase are shown in Figure 9. It can be found that the mixing efficiency was reduced when opening both LRR and SH holes compared to activation of only LRR holes. This is because the downward flow from the LRR was deflected by the jets from the SH (Figure 10b), reducing the momentum directed toward the cold layer. Meanwhile, the buoyancy-dominant flows from SH where the jets were bending upward by the strong buoyancy can be deflected downward by the jets from LRR and thus enhance the pool mixing compared to activation of only SH holes.

The comparison in Figure 11 indicates that the elevation of thermocline with activation of both SH and LRR is between the cases where only one of them opened during the whole transient. However, exceptions can be found if the distance between LRR and SH increases. Two additional conditions can be expected, i.e., (i) two stratified layers are developed if the momentum created by LRR injection is relatively small, developing a thermocline above the SH whereas jets from SH injection develops another thermocline below the SH, (ii) the elevation of the thermocline of opening both holes is lower than activation of any of them if the jets created by LRR are not sufficient to penetrate further than the jets from SH but just enough to further deflect the SH jets downward. In the second way, the pool mixing efficiency is enhanced compared to activation of only one of them.

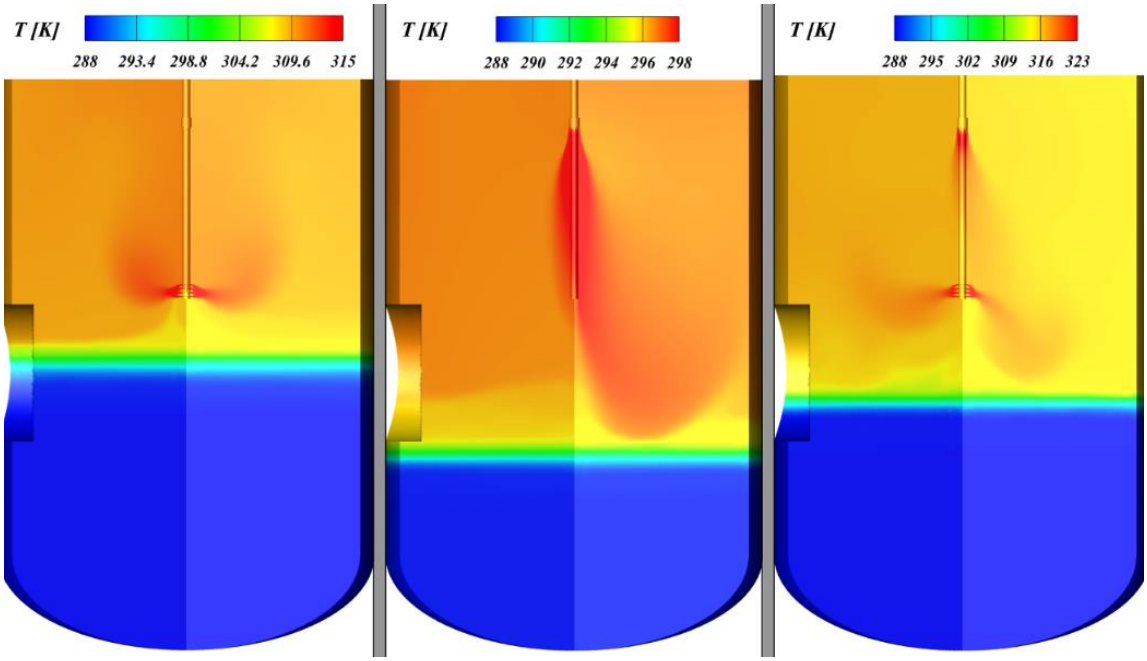

(a) (b) (c)

Figure 9. Temperature contours obtained in cases with opening of (a) SH holes, (b) LRR holes, and (c) SH and LRR holes at $t = 10000s$.

Asymmetry flow patterns and temperature distribution of LRR jets were observed in all injection phases except for phase 1 (Figure 10). It was also reported in previous PANDA LRR tests [40] where the temperature measured from one TC shows higher oscillation and magnitude compared to the one from its mirrored position. These low frequency and high amplitude temperature oscillations were confirmed to be caused by large-scale fluid motions. Later on, CFD simulation provides a good agreement on both temperatures and an asymmetry flow was observed in which the jets induced by LRR injection firstly attached to the sparger pipe and then slightly inclined to the IP side, resulting in an opposite direction compared to the jets in Figure 10b. In current simulations, both inclined directions (either near or far from the IP) are observed and the reason is still unclear. This asymmetry pattern and unpredictable direction will impose difficulty in preparing the PIV plane and possible TCs grid.

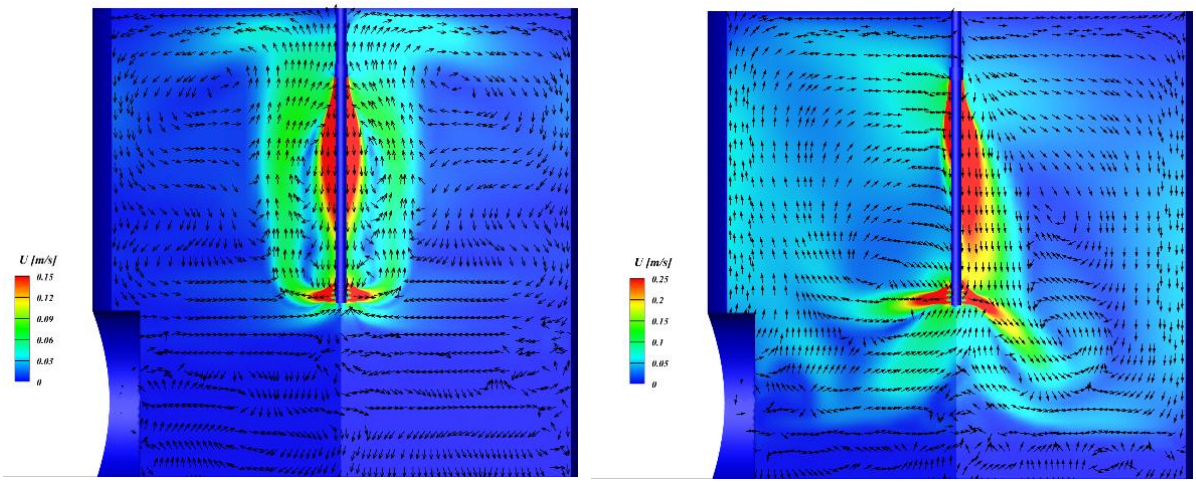

(a) (b)

Figure 10. Velocity contours obtained in case C3 with opening of SH and LRR holes at (a) $t = 6000s$ and (b) $t = 10000s$.

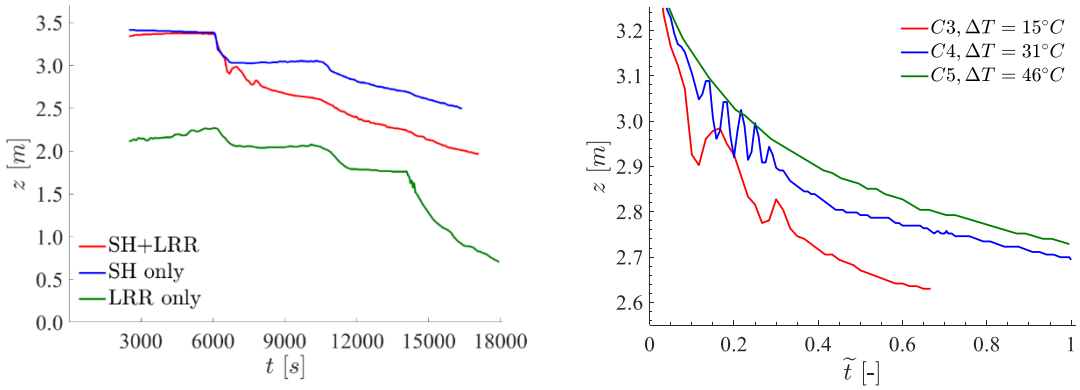

(a) (b)

Figure 11. Comparison of thermocline evolution among cases (a) C1~C3 and (b) C3~C5 at injection phase 2 where $\tilde{t} = (t - t_1)/6000$ (t is the injection time, t_1 the duration in phase 1), ΔT the temperature difference across the thermocline at the end of phase 1 (Figure 12).

3.3.2. Injection procedures

The 6000s injection period in phase 1 created a stratified layer with a temperature difference of ~15℃ (Figure 12). Given the goal of the test is to study the effect of high temperature gradient on the evolution of thermocline, simulations with a longer injection period in phase 1 were performed, resulting in a difference of 31℃ by 12000s duration and 46℃ by 18000s duration. It can be found from Figure 11b that the erosion velocities are reduced when the temperature difference of the thermocline increases. A stronger stratified layer leads to a larger buoyancy force that can resist the vertical momentum to erode the thermocline.

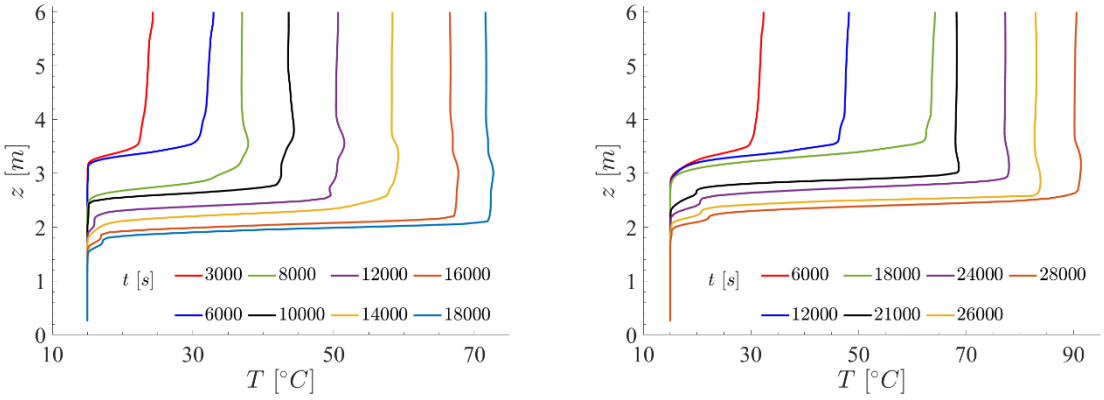

(a) (b)

Figure 12. Vertical temperature profiles in (a) C3 and (b) C5.

The stable or quasi-stable thermocline where the erosion velocity tends to zero was achieved only in the first injection phase (Figure 11a). A 4000~6000s duration seems insufficient for the rest of the phases to develop a stable thermocline. Extending the duration of each phase will lead to a very long overall time and the pool could become saturated. Therefore, we decide to use 4000~8000s for the duration of each injection phase.

By revisiting the main goal and objectives of the P1A6 series (as outlined at the beginning of Section 3), the following tests have been proposed. Their initial conditions and injection procedures are summarized in
Table 3. The motivation for each test is as follows:

- P1A6_1s: Shakedown test
- P1A6_1: Transition from high to low mass flow rates, representing conditions relevant to the plant
- P1A6_2: Investigation of pressure effects, in comparison to the shakedown test
- P1A6_3: Continuous decrease flow rate, representing a plant depressurization scenario
- P1A6_4: Study of erosion effects on a strong thermocline

Table 3. Injection procedures proposed for PANDA P1A6 test series

Test	Initial conditions		Phase 1	P2	P3	P4	P5	P6
	Temperature [℃]	Pressure [bar]	Flow [g/s] (duration [s])					
P1A6-1s	15	1.0	160 (5000)	260 (7000)	360 (8000)	450 (8000)		
P1A6-1	15	1.0	450 (6000)	360 (4000)	280 (4000)	200 (4000)	120 (4000)	40 (4000)
P1A6-2	15	2.0	160 (5000)	260 (7000)	360 (8000)	450 (8000)		
P1A6-3	15	1.0	continuous decrease from 450~0 g/s in ~12000s					
P1A6-4	20(cold) 60(hot)	1.0	260 (6000)	360 (6000)	450 (6000)			

3.4. Pre-test simulations in definition of instrumentations

Velocity measurement plays a significant role in Thermal-Hydraulic (TH) experiments for understanding fluid physics and can be used as the database for the validation of numerical schemes. However, classical measurement approaches employing optical techniques such as PIV are challenging in some applications, particularly in the nuclear industry. In the previous PANDA test, PIV was implemented to measure the flow field induced by steam injection through a multi-hole sparger [32]. The velocities at the middle and far-field regions, where the steam was fully condensed, were recorded when the steam flux was 70 kg/m^2s. However, when the flux was increased to 115 kg/m^2s or even higher, it became impractical to obtain the main flow characteristics due to the rapid collapse of bubbles and significant temperature gradient.

Instead of using PIV, a TC grid arranged by 42 TCs was placed in front of the sparger in PPOOLEX facility as shown in Figure 13. The measured temperature profiles can also reveal the flow characteristics to some extent and the results were then reproduced by CFD simulation using "Unit cell" model where the condensed steam jet was assumed to be a single-phase liquid jet with the same amount of effective momentum. The velocity profiles obtained by using this numerical approach also achieved good agreement with the PIV measurement in PANDA experiments at lower steam flux [44]. The flow after condensation is still a single-phase turbulent flow to which the Reynolds analogy can be applied. This is the oldest and simplest model to estimate the turbulent Prandtl number Pr_t when conducting Reynolds-averaged Navier–Stokes (RANS) simulations. This analogy assumes a similarity between the

transportation of turbulent momentum and turbulent heat transfer in a fluid. In engineering practice, this simple assumption coincides well with experimental data for fluids with $Pr_t \approx O(1)$.

Drawing upon the above discussion, an idea has emerged to reconstruct the flow velocity field by leveraging data from temperature measurements. This concept is particularly relevant in current PANDA experiments where velocity cannot be measured while temperature data can be acquired through a limited number of TCs.

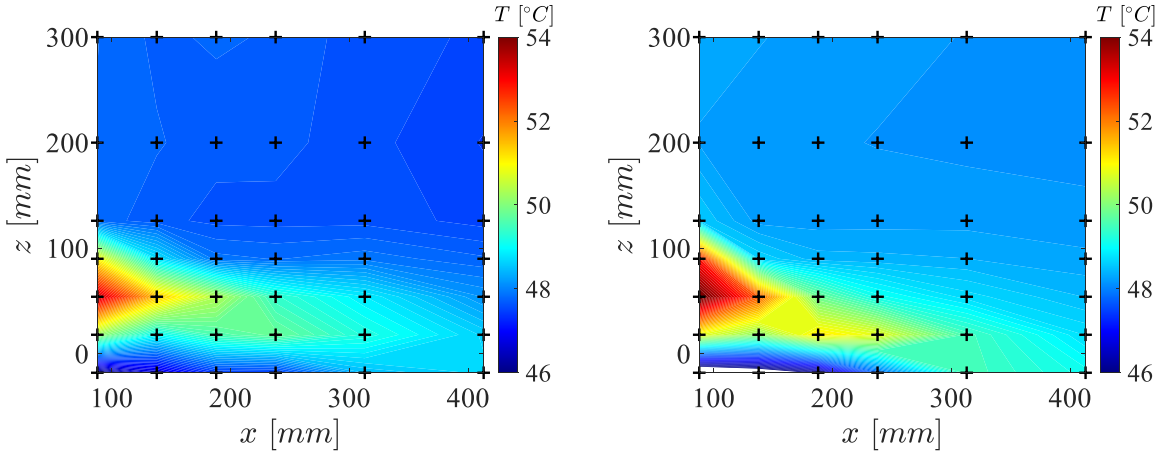

Figure 13. Temperature contours with steam flux of 161 kg/m^2s in PPOOLEX SPA-T3 obtained by (a) TC grid measurement averaged over 100s [3] and (b) simulation using "Unit Cell" model [44]. Symbols (+) correspond to TCs location.

3.4.1. Sparse sensing and field reconstruction

Measurements in containment experiments are normally sparsely collected by sensors, providing limited coverage of the entire domain of interest and being susceptible to both systematic and random noise. The complexity of the steam condensation further limits the feasibility of optical techniques near the injection holes.

Modeling of integral pool experiments (such as PANDA tests) involves numerous Uncertain Input Parameters (UIPs) related to geometry, materials, boundary conditions, many of which are either not directly measurable or have limited accuracy in the experimental measurements. Sensitivity Analysis (SA) is commonly employed to address these uncertainties by identifying the most influential UIPs on specific output quantities, referred to as System Response Quantifies (SRQs). SA improves the efficiency of UIPs calibration by focusing on the most influential ones while the effect of remaining uncertainties is then evaluated by Uncertainty Analysis (UA) [48].

Post-test calibration of UIPs involves comparing simulations with experimental SRQ measurements. SRQs should reflect key physical phenomena and be highly sensitive to UIPs. However, they are often selected based on expert judgment, which may overlook the most sensitive indicators. Since sensors measuring SRQs are sparsely placed, optimizing their locations is essential. This ensures the selected sensors provide data most sensitive to UIP variations, maximizing their usefulness.

The SRQs can be obtained by sparse sensing on the high-dimensional SA dataset as described by Eq. (13) and shown in Figure 14.

$$\boldsymbol{y} = \boldsymbol{C}\boldsymbol{f} \tag{13}$$

where $\boldsymbol{f} \in \mathbb{R}^{n\times m}$ represent the full simulation data across varied UIPs (Figure 14). n is the number of spatial points and m is the number of snapshots. For steady-state simulations, m equals the number of simulations, while for transients, it equals the number of time steps per simulation multiplied by the number of simulations. The SRQ measurements are denoted by $\boldsymbol{y} \in \mathbb{R}^{p\times m}$ collected by p sensors. The measurement operator $\boldsymbol{C} \in \mathbb{R}^{p\times n}$ selects these sensor locations across the domain ($p \ll n$) and is defined as:

$$\boldsymbol{C} = \left[\boldsymbol{e}_{\gamma 1}, \boldsymbol{e}_{\gamma 2} \ldots \boldsymbol{e}_{\gamma p}\right]^T \tag{14}$$

where $\boldsymbol{e}_{\gamma i} \in \mathbb{R}^n$ denotes the canonical basis vectors with a unit entry at index γi (sensor location) and zeros elsewhere.

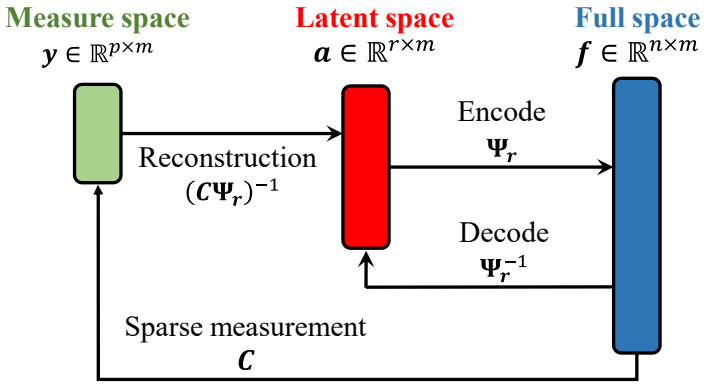

Figure 14. Sparse sensing from high-dimensional space and reconstruction of the latent space.

Nuclear system typically involves millions of grid points, making traditional optimization methods computationally infeasible. Fortunately, the fields of interest often have low-dimensional structures, allowing the use of Reduced-Order Models (ROMs), such as Proper Orthogonal Decomposition (POD), for efficient dimension reduction. These methods compress high-dimensional data into low-dimensional representations with minimal loss of essential features. Thus the SA dataset $\boldsymbol{f}$ can be presented by POD in a low-rank form as:

$$\boldsymbol{f} \approx \boldsymbol{\Psi_r a} \tag{15}$$

where $\boldsymbol{\Psi_r} \in \mathbb{R}^{n\times r}$ is spatial mode matrix where ($r \ll n$) and $\boldsymbol{a} \in \mathbb{R}^{r\times m}$ is coefficient matrix indicating which few modes of $\boldsymbol{\Psi_r}$ are active. These two matrices are solved by data-driven approach using the Singular Value Decomposition (SVD) by Eq. (16) where the leading r left singular vectors consist of the desired POD modes $\boldsymbol{\Psi_r} = u^*_{n\times r}\sum^*_{r\times r}$ (Figure 14).

$$\boldsymbol{f} = u_{n\times n}\sum_{n\times m}v^T_{m\times m} \approx u^*_{n\times r}\sum^*_{r\times r}v^{T*}_{r\times m} \tag{16}$$

Here, '*' indicates ignored submatrices (shown in grey). The matrix $\boldsymbol{f}$ therefore can thus be approximated using lower-dimensional matrices with $r \ll n$. The singular values (diagonal entries of $\sum$) indicate the energy contribution of each mode and guide the choice of truncation

rank. In fluid dynamic systems, the effective degrees of freedom are typically much fewer than the total data dimension, enabling a substantial reduction in r.

With this low-rank representation, the high-dimensional SA dataset can be reconstructed from SRQ measurements using the maximum likelihood estimate of the coefficient matrix, as shown in Eq. (17). This approach is known as gappy POD [49].

$$\hat{\boldsymbol{f}} = \boldsymbol{\Psi_r}\hat{\boldsymbol{a}} = \begin{cases} \boldsymbol{\Psi_r}(\boldsymbol{C\Psi_r})^{-1}\boldsymbol{y}, & p = r \\ \boldsymbol{\Psi_r}(\boldsymbol{C\Psi_r})^{\dagger}\boldsymbol{y}, & p > r \end{cases} \tag{17}$$

where $\hat{\boldsymbol{f}}$ is the reconstructed SA dataset of and $\boldsymbol{f}$, $\hat{\boldsymbol{a}}$ is the estimated coefficient matrix. † denotes the Moore-Penrose pseudoinverse. The estimation is reliable if the number of sensors p is at least equal to the reduced dimension r.

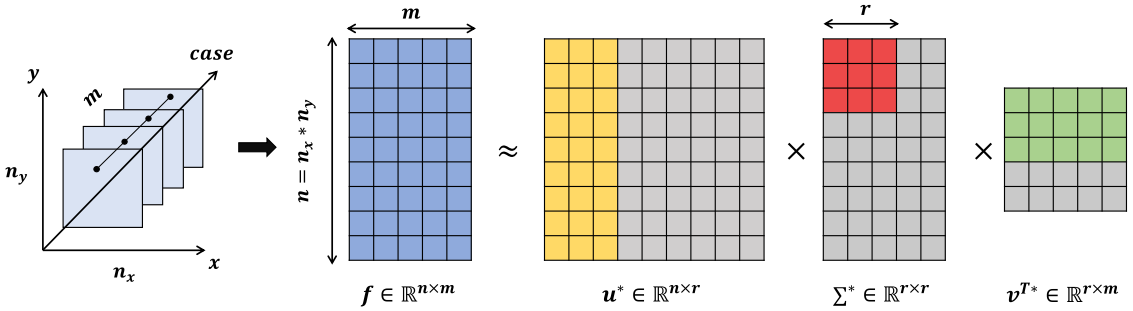

Figure 15. Schematic of dimensionality reduction using POD.

3.4.2. Optimal sensor placement

SRQ selection defines both the type of quantity and sensor locations for experiments. Post-test calibration then adjusts UIPs to minimize the difference between simulated and experimental SRQs. Sensors should be placed to capture measurements highly sensitive to UIP changes. Since $\boldsymbol{f}$ is generated from SA with varying UIPs, optimal sensor placement involves choosing sensor locations that best reconstruct the full field $\boldsymbol{f}$, or equivalently, the mode coefficients $\hat{\boldsymbol{a}}$ i.e. Eqs. (15) and (17).

From Eqs (13)(14)(15), the optimal sensor placement problem can be reformulated to seeks p rows of $\boldsymbol{\Psi_r}$ (sensor locations) that optimally condition inversion of the matrix $\boldsymbol{C\Psi_r}$ as:

$$\gamma_* = \begin{cases} \underset{\gamma}{\operatorname{argmin}} \|(\boldsymbol{C\Psi_r})^{-1}\|, & p = r \\ \underset{\gamma}{\operatorname{argmin}} \left\| \left((\boldsymbol{C\Psi_r})^{\dagger}(\boldsymbol{C\Psi_r}) \right)^{-1} \right\|, & p > r \end{cases} \tag{18}$$

Direct optimization of Eq. (18) is computationally intractable due to the high dimension of the system. The QR pivoting which demonstrates good performance in [50] is applied in this work.

3.4.3. Scoping simulations

Given SA typically involves several UIPs with hundreds to thousands of cases, it is computational impractical for current type of problem where a single transient simulation requires several thousand core hours on a supercomputer. Therefore, we conducted targeted

scoping simulations, focusing on the three most influential UIPs: (i) effective turbulent intensity I_{eff}, and (ii) global filter C_{limit} that determines the additional turbulence induced by steam condensation, and (iii) flow redistribution among the SH and LRR holes. The rationale for selecting these parameters is discussed in Section 3.2 and reference [44]. Table 4 summarizes the values of each varied parameter applied in scoping analysis.

Table 4. List of simulations carried out for second series of pre-test analysis in support of instrumentation designs.

Case No.	Condensation induced turbulence[1]		Flow redistribution[2]	Other variations
	I_{eff}	C_{limit}	δ_{LRR}	
	[-]	[-]	[%]	
C1	2.50	0.10	0	
C2	2.50	0.05	0	
C3	3.25	0.10	0	
C4	3.25	0.05	0	
C5	2.75	0.05	0	
C6	2.75	0.10	0	
C7	2.00	0.10	0	
C8	1.50	0.10	0	
C9	1.00	0.10	0	
C10	0.50	0.10	0	
C11	2.50	0.10	10	
C12	2.50	0.10	20	
C13	2.50	0.10	-10	
C14	2.50	0.10	-20	
C15	2.50	0.10	0	Involvement of sparger support[3]
C16	2.50	0.10	0	3 LRR holes closed[4]
C17	2.50	0.05	0	3 LRR holes closed
C18	2.00	0.10	0	3 LRR holes closed
C19	1.00	0.10	0	3 LRR holes closed

[1] I_{eff} and C_{limit} are parameters determine the condensation induced turbulence introduced in Eq. (12).
[2] Flow rates obtained in Table 1 were varied as: $\dot{m}_{LRR} = \dot{m}_{LRR} + \dot{m}_{LRR}\delta_{LRR}$, $\dot{m}_{SH} = \dot{m}_{SH} - \dot{m}_{LRR}\delta_{LRR}$
[3] Sparger support as shown in Figure 16 was involved in studying its effects.
[4] 3 LRR holes were closed as illustrated in Figure 22 to enforce flow through the TC grid.

Following discussions with the experimental team at the Paul Scherrer Institute (PSI), the sparger elevation was adjusted from 3.7 m (as used in the pre-test simulations in Section 3.3) to 3.05 m to ensure compatibility with other instrumentation, such as PIV laser. Consequently, the pool surface level was lowered from 6.0 m to 5.5 m to facilitate a faster pool heat-up. These modifications were incorporated into this phase of the pre-test simulations. The objective of these simulations is to support the design of instrumentation, including the arrangement of thermocouples (TCs) and the positioning of the PIV field of view (FOV).

All simulations were conducted with a initial pool temperature of 15℃ and pool pressure of 1 bar. The pool was pressuzied and the steam injection was proceeded as: (i) phase 1:160g/s by

5000s (ii) phase 2: 260g/s by 7000s (iii) phase 3: 360g/s by 8000s (iv) phase 4: 450g/s by 8000~12000s.
Both LRR and SH holes were activated except for C16 to C19 where 3 LRR holes were closed as illustrated in Figure 22 to enforce the flow passing through the TC grid. This is because that asymmetric flow pattern was observed in previous PANDA H2P3 tests when steam was injected through LRR holes with a symmetry configuration and such flow pattern is unstable [47]. This asymmetric behavior is also evident in pre-test analysis as shown in Figure 10.

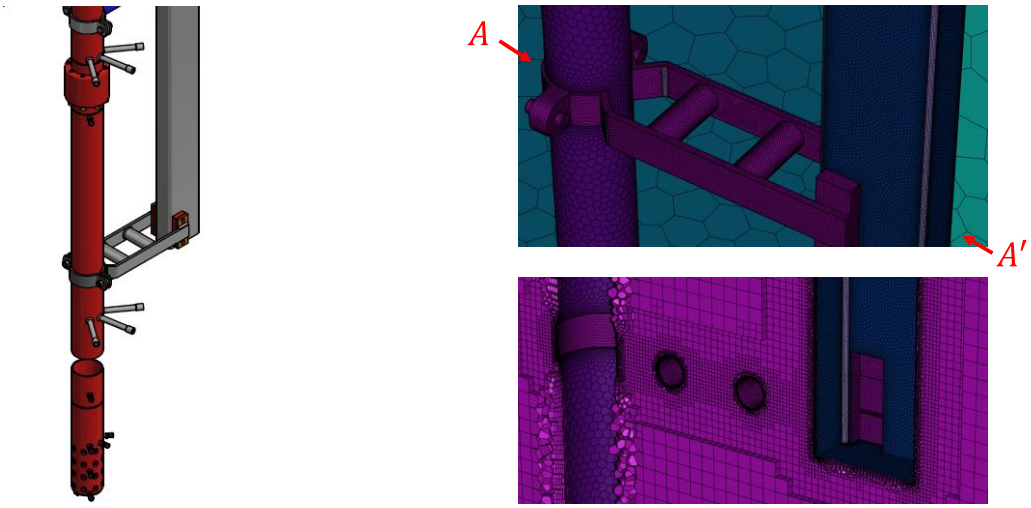

Figure 16. (a) Schematic of sparger support and its (b) mesh in scoping analysis summarized in Table 4.

Figure 17 presents the temporal evolution of pool temperature in a representative scoping simulation. The results indicate that the proposed steam injection procedures is sufficient to achieve a near-saturated pool condition by the end of the test. The thermal stratification interface descends progressively as the steam flow rate increases. These temperature profiles were then used to determine the elevation of the stratified layer through its gradient along the vertical direction. The outcomes for selected cases are compared in Figure 18.

The parametric study demonstrates that thermal stratification of the pool is maintained under the current injection conditions, even when accounting for model uncertainties. The presence of the sparger support structure as shown in Figure 16 has a negligible effect on overall pool behavior. In contrast, pool response is highly sensitive to the flow distribution between the SH and LRR holes. Thus, accurate measurement of these flow rates is essential during the tests.

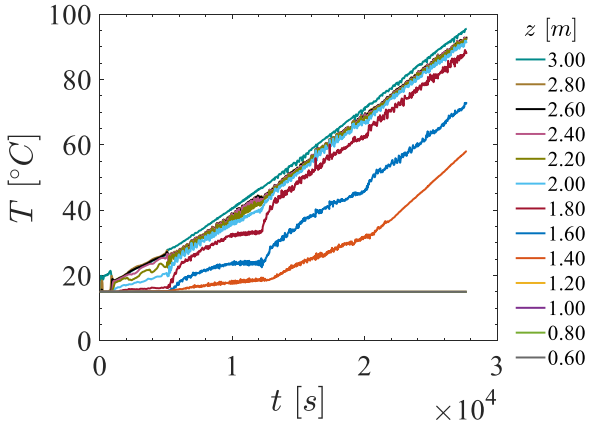

Figure 17. Temperature evolution obtained from scoping simulation of C1 (Table 4).

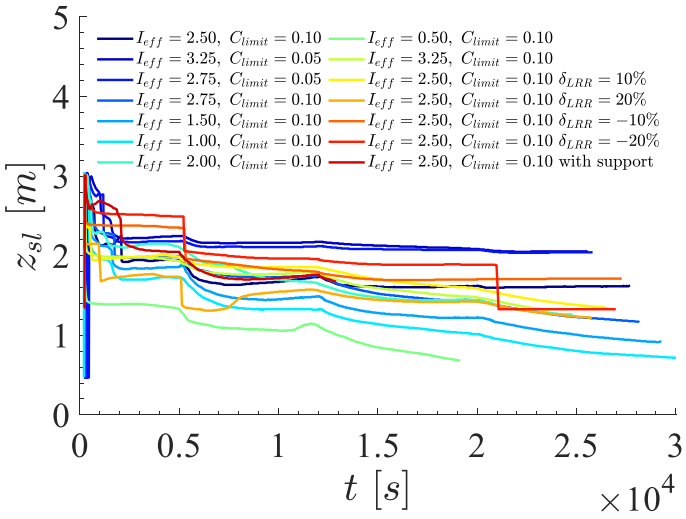

Figure 18. Thermocline evolutions obtained from selected scoping simulations as summarized in Table 4.

3.4.4. Design of instrumentation

The results of the scoping simulations (Table 4) were combined to determine TC locations via the optimal sensor placement approach as introduced in Sections 3.4.1 and 3.4.2. For each case, temperature and velocity fields were sampled to form the full state matrices $\boldsymbol{f}_T$ and $\boldsymbol{f}_U$ (Eq. (13)). Each matrix had dimensions 96913×2463, constructed from 2463 snapshots (each containing 96913 nodes) extracted from 19 transient simulations (Table 4), with 60–150 snapshots per run sampled at 100–200 s intervals. We formed the fluctuating dataset $\boldsymbol{f} = \boldsymbol{f} - \bar{\boldsymbol{f}}$, where $\bar{\boldsymbol{f}}$ is the temporal mean of each matrix. The dataset was split into training (85%) and testing (15%) subsets to fit (Eqs. (15)–(17)) and evaluate the model performance, respectively.

Optimal sensor placement was performed on both fields via QR pivoting to solve the Eq. (18) [50]. As shown in Figure 19(a), 6 temperature sensors suffice to reconstruct $\boldsymbol{f}_T$ with a cumulative variance of 0.99, i.e. 99 % of the information is retained. Conversely, reconstructing $\boldsymbol{f}_U$ requires 19 velocity sensors (Figure 19(b)), reflecting its more complex spatial-temporal behavior. In both cases, optimal locations cluster around the injection holes, where the results are sensitive to the UIPs.

However, the deployment of velocity sensors is impractical in the current PANDA facility. According to Reynolds' analogy, which assumes a similarity between turbulent momentum transport and turbulent heat transfer, we propose a combined placement by replacing all velocity sensors with temperature sensors (Figure 19(c)). Recognizing that TC installation requires additional mounting infrastructure, we further propose two compact configurations: (i) "Proposal A" based on the PPOOLEX TC grid (Figure 13) configuration (Figure 19 (d)), and (ii) "Proposal B" based on the combined optimal locations in temperature $\boldsymbol{f}_T$ and velocity $\boldsymbol{f}_U$ fields (Figure 19 (e)). In addition, five random thermocouple configurations were generated for comparison, one of which is illustrated in Figure 19 (f).

The optimality of various sensor configurations was evaluated by comparing their reconstruction errors, specifically the Normalized Mean Square Error (NMSE), on the testing dataset. The reconstruction is performed using Eq. (17), in which $\boldsymbol{y}$ denotes the sparse temperature measurements provided by the TCs.

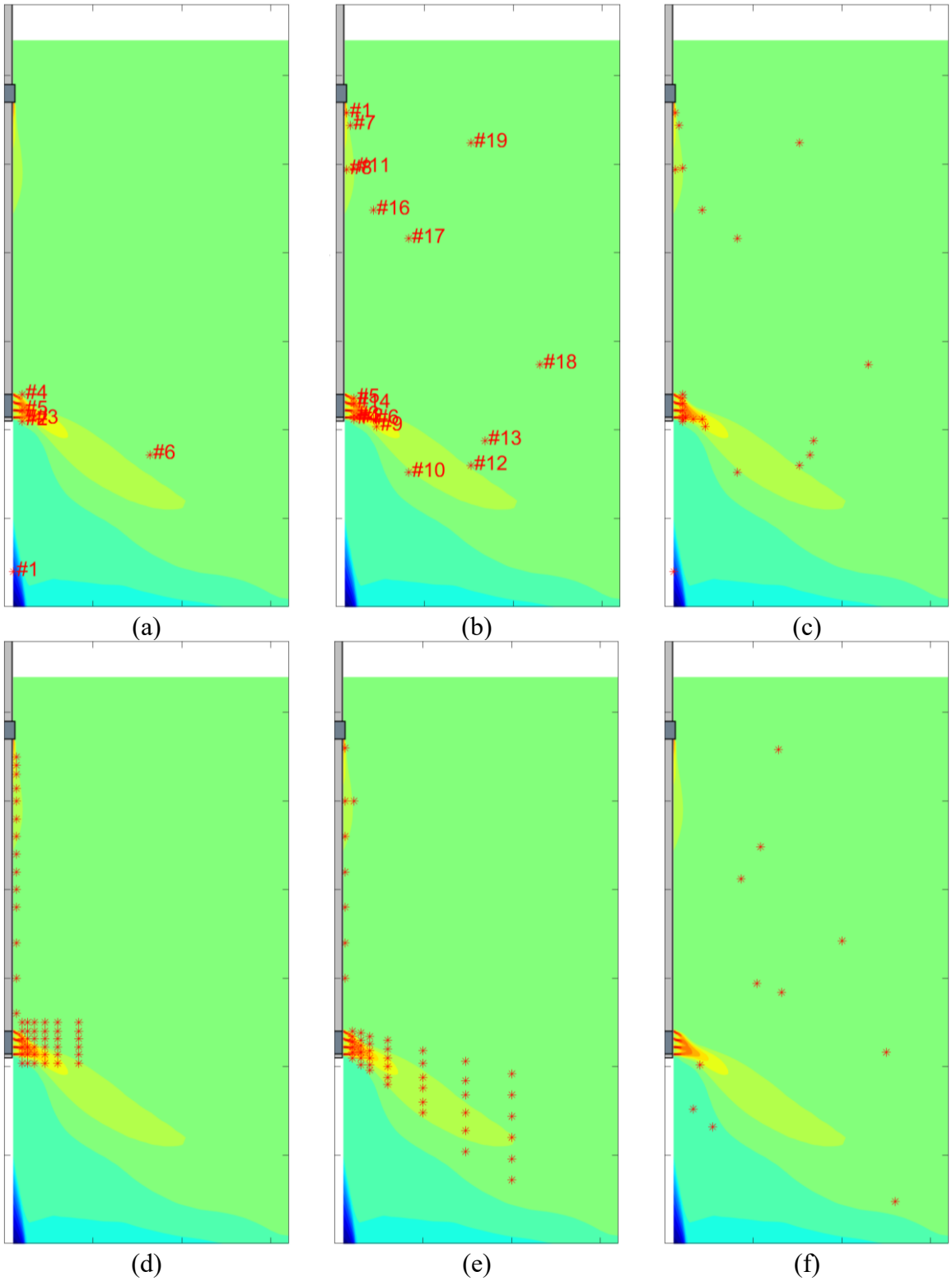

Figure 19. Thermocouple (TC) locations: (a) optimal placement based on the temperature field $\boldsymbol{f}_T$; (b) optimal placement based on the velocity field $\boldsymbol{f}_U$; (c) combined sensor locations from (a) and (b); (d) "Proposal A," based on the PPOOLEX TC-grid configuration (Figure 13); (e) "Proposal B," based on the combined optimal locations in (a) and (b); and (f) one of five randomly generated distributions. Locations displayed on a temperature snapshot at high steam flow rate.

Reconstruction performance is expected to degrade in the presence of noise measurement. In our context, noise comprises (1) an inherent fluctuation of approximately 0.1 K arising from electrical signal oscillations, and (2) a fixed offset, varying between 0.1 K and 2 K during the test (which can be largely mitigated by calibration test). Moreover, discrepancies in sensor positioning during experiments may also introduce noise.

To assess the robustness of each design, we contaminated the sparse temperature inputs with Gaussian noise $N(0, \sigma^2)$, varying σ^2 from 0 to 2. Six sensor arrangements as shown in Figure 19 were examined and the results are summarized in Figure 20. The combined optimal placement (Optimal T+U sensors) consistently yields the lowest reconstruction error and remains the most stable as noise increases. Other designs maintain comparable accuracy for $\sigma^2 \leq 0.5$, but the errors of random distributed sensors escalate rapidly at higher noise levels. Notably, the proposals A and B demonstrate that the compact, engineering-practical TC grid can perform nearly well as the optimal design. These findings highlight that optimized sensor placement is essential during pre-test analysis.

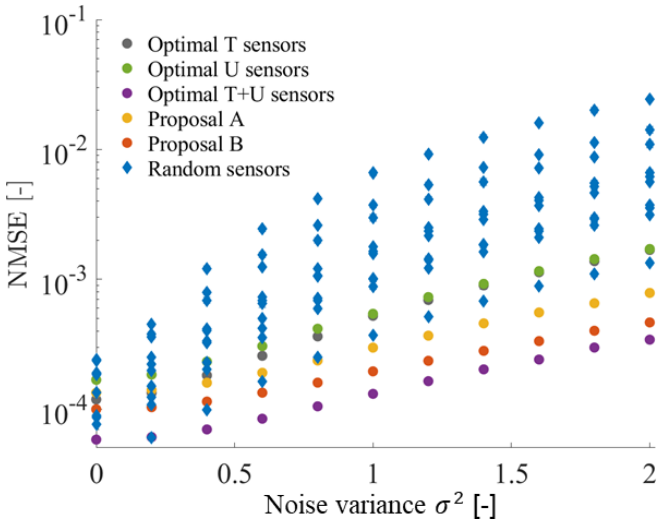

Figure 20. Error of reconstruction of full state temperature by sparse sensor results polluted by noise. Cases compared with different sensor arrangements as shown in Figure 19.

Given that proposal B provide a broader coverage of the thermal field (Figure 21), it is selected for implementation in the PANDA P1A6 tests. The final design of the TC layout is illustrated in Figure 22. Besides the TC grid designed in this section, the TCs as applied in previous PANDA tests (Figure 3) are retained.

The final layout places the PIV FOV immediately adjacent to TC grid, but not co-planar with a small distance and oriented in parallel allowing nearly simultaneous measurement of velocity and temperature in the same region but with a overlap on their projection. This arrangement ensures that the TC grid can capture flow details near the injection holes where PIV is challenging, while the PIV provides velocity measurement at far field. Such measurements offer the opportunity to reconstruct the missing information (obscured by steam condensation) using data assimilation approaches such as Physics-Informed Neural Network (PINN). The reconstructed flow fields are expected to provide more reliable estimates of momentum and heat transport in the vicinity of the sparger, offering valuable databases for the development and validation of mechanistic models.

The final layout places the PIV FOV immediately adjacent to the TC grid in a parallel plane separated by a small gap (Figure 22), providing a nearly simultaneous measurement of velocity and temperature in the same region. In the vicinity of the sparger, where using PIV is challenge, the TC grid provides robust temperature data. Further downstream, the PIV records velocity fields in the far field. These synergic measurements make it possible to recover information obscured by steam condensation through data assimilation techniques such as physics-informed neural networks (PINNs). The resulting high-fidelity velocity and temperature fields will yield more reliable estimates of momentum and heat transport around the sparger and will serve as a valuable benchmark for the development and validation of mechanistic models.

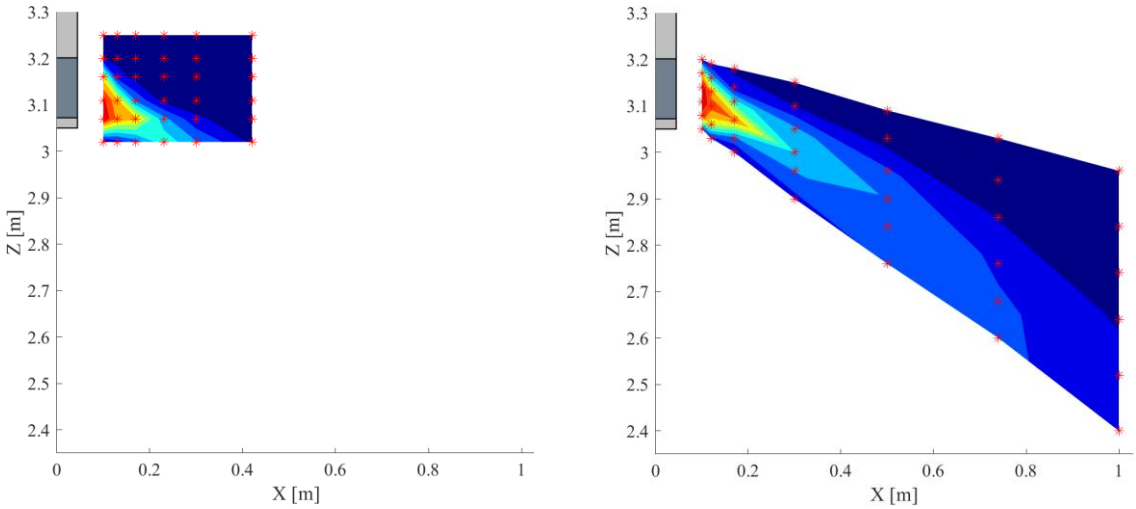

Figure 21. Temperature contours obtained by linear interpolations among sparse temperature measurements with (a) 'Proposal A' and (b) 'Proposal B'. Sensors are indicated by *.

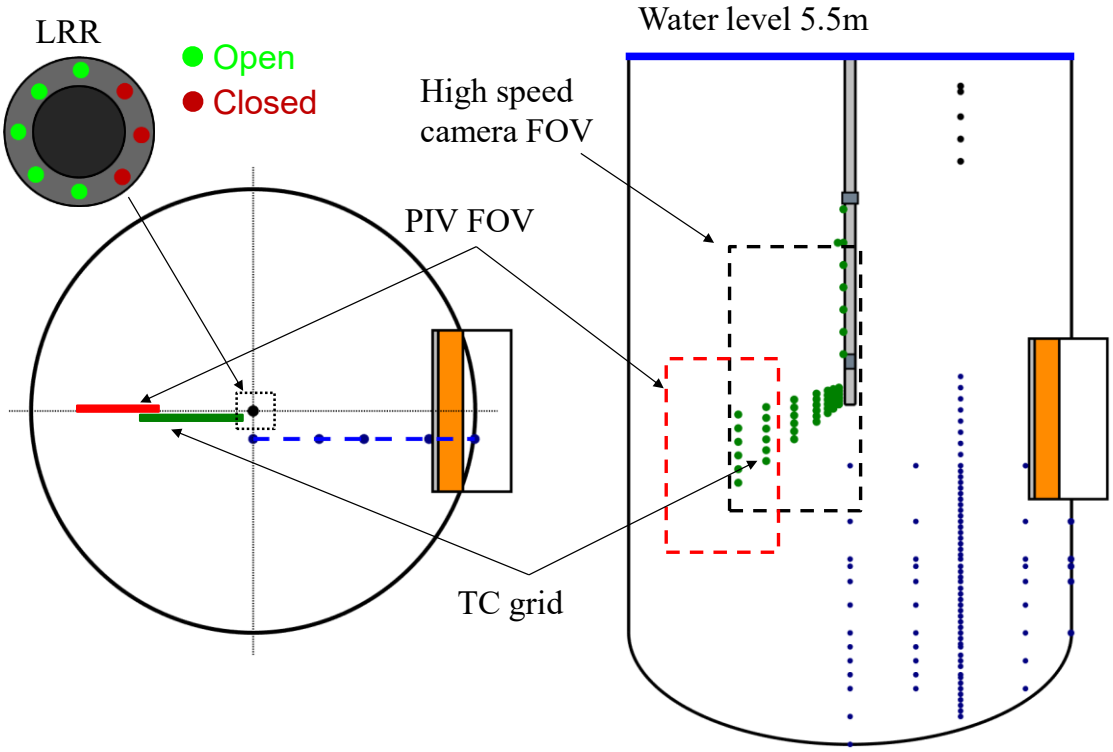

Figure 22: Instrumentations of PANDA facility designed for P1A6 sparger tests.

4. REVIEW OF METHODOLOGY FOR ANALYSIS OF PASSIVE SAFETY SYSTEM RELIABILITY

In this section, we review the most recent developments in the field of passive safety system (PSS) reliability analysis. Based on a synthesis of literature, key knowledge gaps are identified to guide future methodological improvements. Section 4.1 outlines the significance of reliability analysis for Passive Safety System (PSS), Section 4.2 introduces the general framework and key steps involved in such analyses. Section 4.3 provides a brief summary of the state-of-the-art methodologies, and Section 4.4 discusses the associated challenges and unresolved knowledge gaps.

4.1. Importance of reliability analysis for PSS

Reliability is defined as the probability that a system or component will fulfill its minimum performance requirements when required to do so, over a specified period and under specific operating conditions. In the context of nuclear power plant design, reliability assessment is a critical aspect in determining and ensuring that PSS can perform their intended safety functions with the required degree of confidence.

In the case of active safety systems, reliability is typically ensured through the implementation of redundant components, robust engineering design, high quality components, and rigorous programs for functional testing, qualification and maintenance. Failures in such systems are usually linked to identifiable mechanical or electrical malfunctions, commonly known as active failures. These failures are often detectable during scheduled maintenance or routine testing, allowing for timely correction.

On the other hand, PSS rely on intrinsic physical mechanisms and generally do not involve moving parts once initiated. As a result, they are less vulnerable to conventional hardware-related failures. Nevertheless, they are still at risk of experiencing what is termed as functional failure or phenomenological failure—a form of system-level malfunction that may occur without any damage to physical components. This type of failure stems from the system's dependence on weak driving forces and its high sensitivity to variations in environmental and boundary conditions, which can reduce its ability to perform the intended safety function. In many instances, such deviations from design assumptions can cause performance degradation despite fully intact hardware.

A critical challenge in evaluating PSS reliability lies in the uncertainty associated with the wide range of operational states and initiating conditions that a passive system may experience. Certain combinations of internal and external influences can impose thermal-hydraulic loads that exceed the system's design capacity or compromise its safety margins, potentially leading to functional failure.

Key contributors to such failures may include:

- Accumulation of non-condensable gases.
- Presence of undetected leaks.
- Excessive heat losses.
- Inefficient piping arrangements.

- Limited valve opening area in discharge lines.
- Obstruction or fouling within heat exchangers.

Understanding this failure mode requires comprehensive deterministic and probabilistic analysis to identify the scenarios under which the system may not behave as intended. Therefore, the development and use of appropriate modeling and assessment methodologies are critical.

4.2. General steps for analysis of PSS reliability

The section presents a systematic methodology for assessing the reliability of PSS in the presence of complex scenario interactions and coupled phenomenological processes. Its structure draws on the framework described in the Electric Power Research Institute (EPRI) report [51].

The reliability analysis of a PSS proceeds through five steps:

1. Establishing the need for comprehensive PSS analysis.
2. Collecting information on the PSS design from all available sources
3. Identifying relevant accident scenarios.
4. Conducting phenomenological analysis of the PSS, to identify potential failure modes.
5. Quantifying PSS reliability.

Comprehensive PSS analysis is required when either the failure of the PSS is of high-risk importance or the uncertainty in the evaluation of the functional margin and/or risk significance is large. The later situation arises if potential failure modes are poorly understood or highly variable, if scenarios are so complex that they challenge system reliability, or if the PSS interacts significantly with other active or passive systems. It can also be caused by the lack of well validated mechanistic models for describing relevant complex phenomena.

A comprehensive analysis requires careful collection of information on the PSS system design and importantly on the coupled systems. Some of the data may have to be generated through phenomenological calculations. The following types of information have to be collected, including (i) system performance, (ii) hardware component data, (iii) maintenance data, (iv) support system data, (v) phenomenological calculations and experimental data, (vi) expert elucidation, etc.

The next step is to identify potential PSS failure modes which require a broad search of all possible scenarios and operational occurrences. The ultimate objective is to identify scenarios which can challenge the operation of the passive safety system. For each scenario, its frequency and the conditional probability of PSS failure are preliminarily assessed. Examples of the cases span external events (e.g., loss of off-site power), internal malfunctions (e.g., actuation signal failures), phenomenological degradations (e.g., reduced heat-removal capacity) and its interactions with other systems.

At this stage, scenario and failure mode identification relies primarily on expert judgment. However, due to the complexity and interdependence of initiating events, failure mechanisms, and their respective failure modes, this step is inherently uncertain. To enhance the robustness and traceability of the analysis, it is essential to explicitly define the assumptions used to constrain the scenario space. Sensitivity analyses should be employed to justify and validate these limitations.

After identification of the scenarios, phenomenological analysis is needed to identify failure modes of the PSS. EPRI report which was written almost 20 years ago recommends limiting the number of phenomenological calculations to arrive to an acceptable estimate of PSS reliability sufficient for decision making within PRA. However, at the present stage, huge (in 2008 terms) computational resources can be readily available for an individual analyst. Therefore, it would be much more prudent to reduce the "user effect" in the describe above approach through the means of automated search for the failure modes in the space of selected accident scenarios. This stage should include a rigorous evaluation of parameter importance, modeling uncertainty, and code-specific uncertainties. A comprehensive methodology relaying on sensitivity analysis and uncertainty quantification has to be applied (e.g., refer to Section 4.3).

The final stage is to quantify the PSS reliability. It commonly requires data on frequency of considered scenarios and estimated conditional probability of the PSS failure. Scenario dependent combinations of these two values can be used to support decision on PSS reliability as illustrated in Figure 23.

Two scenario frequency thresholds are commonly applied in this context:

(i) scenarios with frequencies over 10^{-3} per year are considered to occur too often to impact the reactor safety and it should be eliminated,

(ii) scenarios with frequencies under 10^{-6} per year are considered to be unrealistic and marginal.

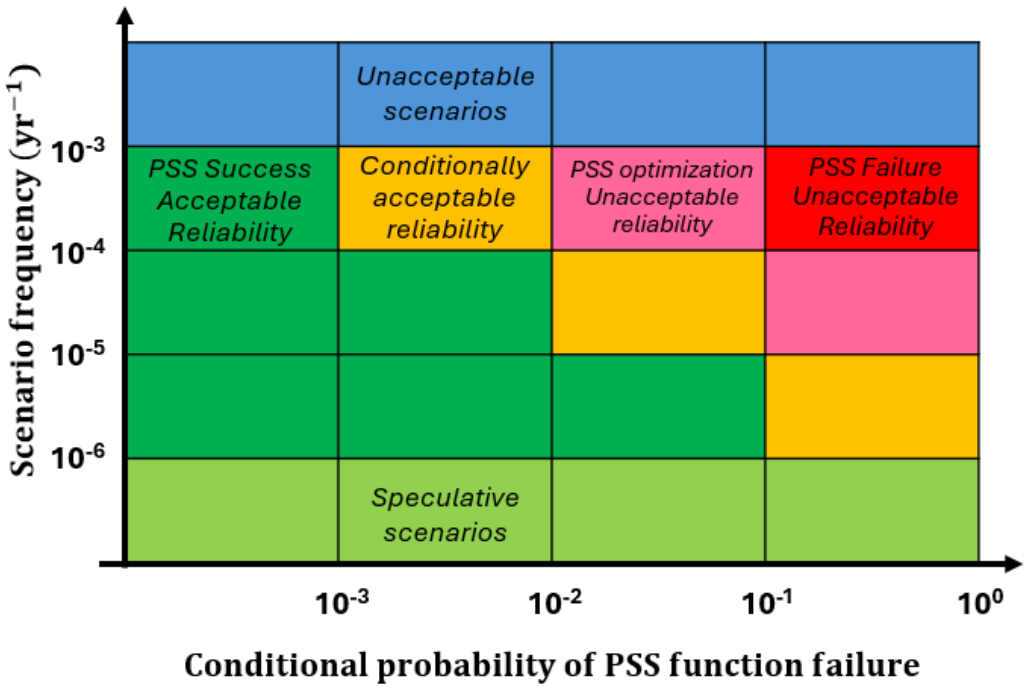

Figure 23: Assessment of PSS reliability

4.3. Summary of reviewed methodologies

This section presents a summary of four major methodologies that represent the current state-of-the-art for evaluating passive system reliability in nuclear reactors, especially SMRs. Each methodology reflects a distinct balance between deterministic and probabilistic elements, computational demands, and applicability to different failure modes (functional vs. hardware-related). A detailed review can be found in [51].

4.3.1. **REPAS:** Reliability Evaluation of Passive Safety Systems

The REPAS methodology is a comprehensive analytical framework developed to evaluate the thermal-hydraulic reliability of PSS, particularly those governed by passive features such as natural circulation, condensation, and gravity-driven flows [53, 54, 55, 56]. Although initially designed for passive systems, REPAS has also been successfully applied to active safety systems.

REPAS aims to rigorously quantify the reliability associated with the passive systems by analyzing the variation of thermal-hydraulic behavior under uncertain boundary and operational conditions. It serves several objectives: (i) increase confidence in the reliability of PSS operation, (ii) compare alternative passive or active system configurations, (iii) establish robust design margins through quantified performance indicators.

REPAS integrates deterministic thermal-hydraulic modeling with probabilistic techniques, relying on: (i) Fault Tree (FT) and Event Tree (ET) logic to identify and structure failure mechanisms, (ii) Wilks' formula [57, 58] to determine the statistically enough simulations (code runs) required for confidence-bound estimation of system reliability. The main Figure of Merit (FOM) generated by REPAS are: (i) the probability of functional failure, i.e., the likelihood of FC violation under varying input conditions; (ii) Parameter impact metrics, quantifying the contribution of uncertainties to FOM variability.

The REPAS methodology consists of a multiple steps structured workflow (Figure 24):

1. **System selection & mission definition**: Define the passive system and its Target Mission (TM), along with the key thermal-hydraulic phenomena involved in mission fulfillment.
2. **Definition of Failure Criteria (FC)**: Set specific thresholds or time-dependent functions to characterize system failure. These may include static or integral metrics (e.g., maximum cladding temperature, IC heat transfer integral).
3. **Identification of Failure Mechanisms/Modes**: Apply systematic tools (ET/FT) to exhaustively identify hardware, phenomenology, or environmental causes of failure.
4. **Phenomenological decomposition**: Break down key processes into fundamental physical parameters (e.g., pressure drops, flowrates, heat fluxes).
5. **Parameter classification & reduction**: Classify parameters by importance and reduce the dimensionality of the problem for computational efficiency (e.g., filter non-dominant parameters).
7. **Parameter dependencies**: Identify and encode physical or statistical dependencies between parameters (e.g., pipe diameter vs. flow regime).
8. **System modeling**: Develop a detailed thermal-hydraulic model (e.g., using RELAP5, TRACE) to simulate system transients.
9. **Deterministic reference simulation**: Run a best-estimate simulation under nominal conditions to establish a performance benchmark.

10. **Probability distribution assignment**: Assign probability distributions or discrete probabilities to each uncertainty parameter, reflecting both epistemic and aleatory uncertainties.
11. **Uncertainty propagation**: Use stochastic sampling (e.g., Latin Hypercube, Monte Carlo, or Wilks' method) to run an ensemble of *N* simulations covering the plausible parameter space.
12. **Reliability evaluation**: Compare each of the *N* transient simulation outcomes against the FCs. Calculate the probability of failure as the fraction of simulations that violate the criteria, and correlate results with parameter variations to identify sensitivity.

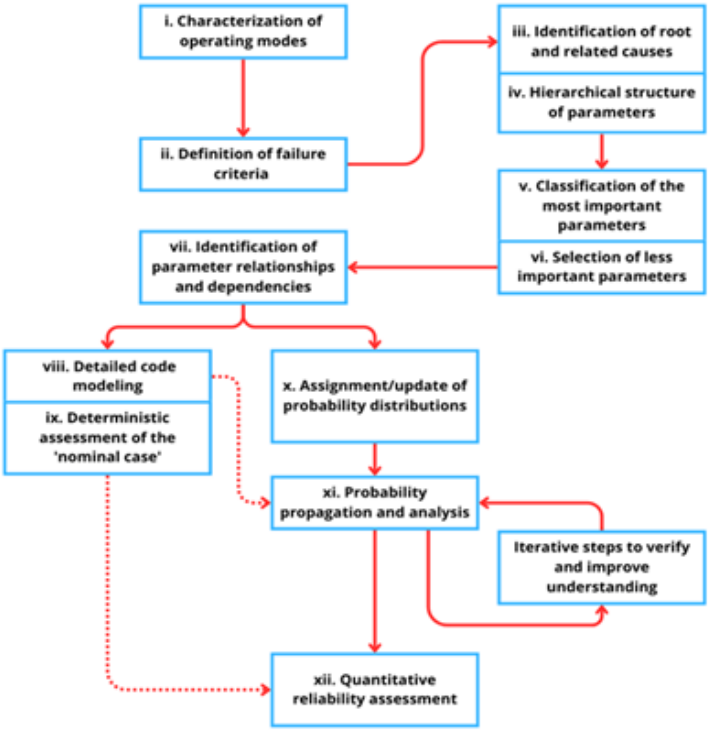

Figure 24: The workflow of REPAS [54, 56].

REPAS offers rigorous treatment of uncertainty via statistically bounded ensemble simulations, and it is suitable for both passive and active systems, with flexible integration into the Probabilistic Safety Assessment (PSA) frameworks. However, it is limited by intensive calculations especially when multiple FOMs and large parameter spaces are involved. Moreover, Reliability estimates are sensitive to the quality of input distributions and failure criteria definitions.

4.3.2. **RMPS**: Reliability Methods for Passive Systems

The **RMPS** methodology is a structured probabilistic framework developed under the European 5th Framework Program to assess the assess the reliability of passive safety functions in industrial systems, primarily in nuclear applications [58]. Though originally tailored for nuclear systems, RMPS has been extended to other high-risk industries such as chemical, oil, and gas sectors. It is particularly well-suited for analyzing systems where complex thermal-hydraulic phenomena and uncertainty quantification are critical to safety assurance.

The RMPS process follows a sequential six-stage roadmap (Figure 25):

1. **System characterization**: Define the system mission, operational scenario (e.g., LOCA, SBO), potential failure modes, and establish clear success/failure criteria based on physical indicators (e.g., cladding temperature thresholds, system pressure limits).
2. **System modeling**: Develop a **best-estimate thermal-hydraulic model** using validated codes (e.g., CATHARE, RELAP5). The model is tested and benchmarked against reference transients or experimental results, and its limitations are documented.
3. **Parameter identification**: Screen and select influential parameters using sensitivity studies or expert judgment.
4. **Uncertainty quantification**: Assign probability distributions to the selected parameters. Where experimental data or operational experience is unavailable, distributions are typically based on expert judgment.
5. **Uncertainty propagation**: Apply Monte Carlo or surrogate based methods to propagate the uncertainty space. Surrogate Models (SM), e.g., polynomial response surfaces, gaussian process regression, neural network, are often employed to reduce computational burden while maintaining fidelity to the underlying physics.
6. **Reliability Evaluation**: Evaluate system failure probability by analyzing simulation outcomes against the predefined failure criteria. The output includes a quantitative measure of reliability and insights into parameter sensitivity.

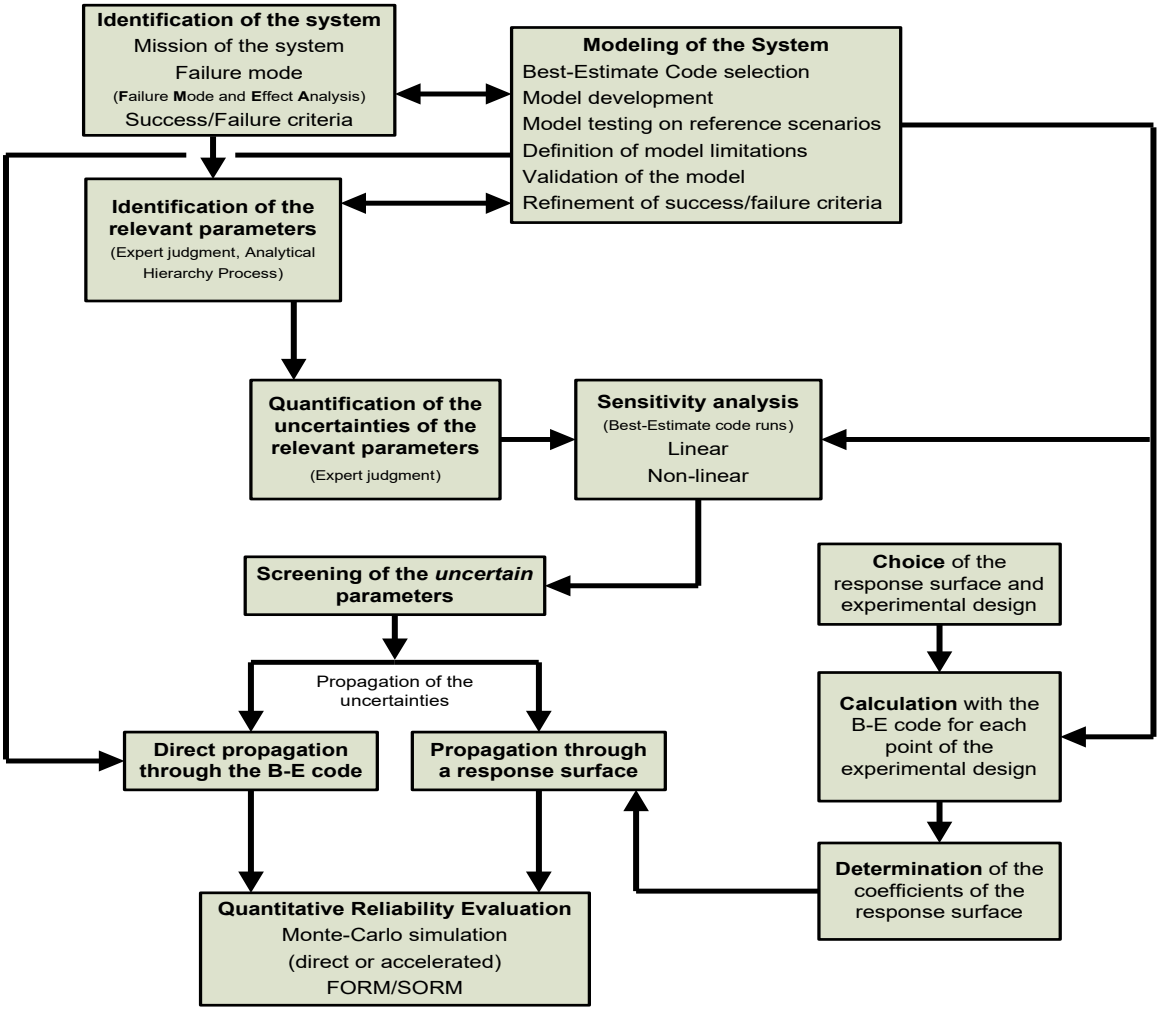

Figure 25: The workflow of RMPS [59].

The RMPS methodology offers several notable advantages that contribute to its credibility and relevance in PSS reliability assessment. It enables a realistic treatment of uncertainty by incorporating the full variability of input parameters through probabilistic sampling. The methodology has demonstrated broad applicability across various PSS and reactor types, establishing its versatility. Furthermore, the integrated sensitivity and uncertainty analyses provide valuable diagnostic insight into which parameters most significantly affect system reliability, thereby informing both design optimization and safety justification.

One primary limitation of RMPS is the modeling uncertainty and user effect, as the fidelity of the thermal-hydraulic model plays a critical role in the accuracy of the results. The selection of nodalization schemes, modeling assumptions, and user expertise can introduce variability that affects the final reliability estimate. As a result, many parameter uncertainties must be derived from expert judgment, which introduces subjectivity into the process.

Another significant limitation is the computational cost. When estimating small failure probabilities (e.g., on the order of 10^{-6}), direct Monte Carlo simulation may require an exceptionally large number of simulations—often in the millions—to achieve statistically meaningful results. The required large number of model runs, increases as the inverse of the failure probability and the square of the acceptable fractional error. For systems with complex dynamics and long simulation times, such computational demand becomes prohibitive. In such cases, the use of SMs is essential to reduce simulation time while preserving prediction accuracy.

Lastly, the scenario-specific nature of RMPS results presents another challenge. Since the methodology must be applied independently for each transient scenario or initiating event, the overall workload increases significantly when a comprehensive range of plant conditions needs to be evaluated.

4.3.3. **APSRA**: Assessment of Passive System Reliability

The APSRA methodology is developed by the Bhabha Atomic Research Centre (BARC) [61].

This approach assesses PSS reliability by estimating the probability that the system will fail to perform its intended function, attributing such failure to deviations in key parameters caused by mechanical component malfunctions (e.g., valves, rupture discs, control systems). These deviations are analyzed using thermal-hydraulic simulations (e.g., RELAP, ATHLET, MELCOR) to generate a failure surface. A root-cause analysis is then conducted to identify the underlying component failures, and their probabilities are quantified using standard PSA techniques such as fault tree or success tree analysis.

The process includes the following steps (Figure 26):

- **Identification of the passive system:** Select the passive safety system of interest and define the objective of the analysis. This includes understanding the system's intended function during specific operating or accident scenarios.
- **Identification of influential parameters**: Determine the key operating parameters that significantly impact the passive system's performance. For example, in natural circulation systems, parameters may include system pressure, heat input, feedwater temperature, subcooling, water level, or the presence of non-condensable gases.
- **Characterization of operational behavior and failure criteria**: Analyze how the system is designed to function and establish specific criteria that define failure. These

criteria may relate to temperature, pressure, flow rate, or other performance metrics. At this stage, simplified engineering analyses or low-fidelity simulations may be sufficient to understand qualitative behavior.

- **Identification of critical parameters leading to failure**: Based on the system's behavior and failure criteria, identify which parameter deviations are most likely to cause a functional failure. Distinguish between critical and non-critical variables using engineering judgment or preliminary sensitivity analysis.
- **Generation of the failure surface:** Perform a series of best-estimated thermal-hydraulic simulations (e.g., with RELAP5, ATHLET, MELCOR) to map out the combinations of critical parameter deviations that result in failure. This defines the system's failure surface or failure boundary in the input parameter space. Validation with experimental data is encouraged to reduce modeling uncertainty.
- **Root-cause diagnosis of parameter deviations**: Conduct a root-cause analysis to determine how deviations in critical parameters could arise. This involves identifying mechanical component failures that could lead to the deviations mapped on the failure surface.
- **Evaluation of component failure probabilities:** Estimate the failure probabilities of the components identified in Step VI using classical PSA methods. This may involve using fault trees, success trees, or reliability databases with either generic or plant-specific failure data.
- **Evaluation of PSS reliability:** Integrate the component failure probabilities into a fault tree model where the top event represents the passive system's functional failure. The final output is the system-level reliability metric, derived from the combination of lower-level hardware failures that influence passive system performance.

While the APSRA methodology addresses a similar domain as RMPS—namely, the reliability evaluation of PSS—it differs significantly in its conceptual approach and technical implementation. APSRA focuses on identifying mechanical component failures as the root cause of deviations in key process parameters that lead to system failure [60]. These component failures are then incorporated into a PSA model, typically using fault tree analysis. However, APSRA does not consider that physical processes themselves may fail probabilistically; it assumes such failures only occur when their enabling conditions are disrupted by hardware malfunctions.

Unlike RMPS, which treats parameter variations and model uncertainties uniformly through probability distributions, APSRA distinguishes between them. It attributes parameter variability to functional failures of supporting systems and relies on experimental validation to estimate model uncertainty. In the absence of data, APSRA does apply probability distributions, but these are introduced only after failure probabilities are estimated from parameter deviations. Additionally, while RMPS employs Monte Carlo simulations for reliability quantification, APSRA constructs a failure surface and evaluates system reliability using deterministic PSA techniques.

One notable limitation of APSRA is that it does not prescribe specific methods for quantifying component failure probabilities, which are critical to the overall assessment. Instead, it allows the use of either generic or plant-specific reliability data but does not incorporate advanced statistical approaches such as Bayesian updating to combine multiple sources of evidence.

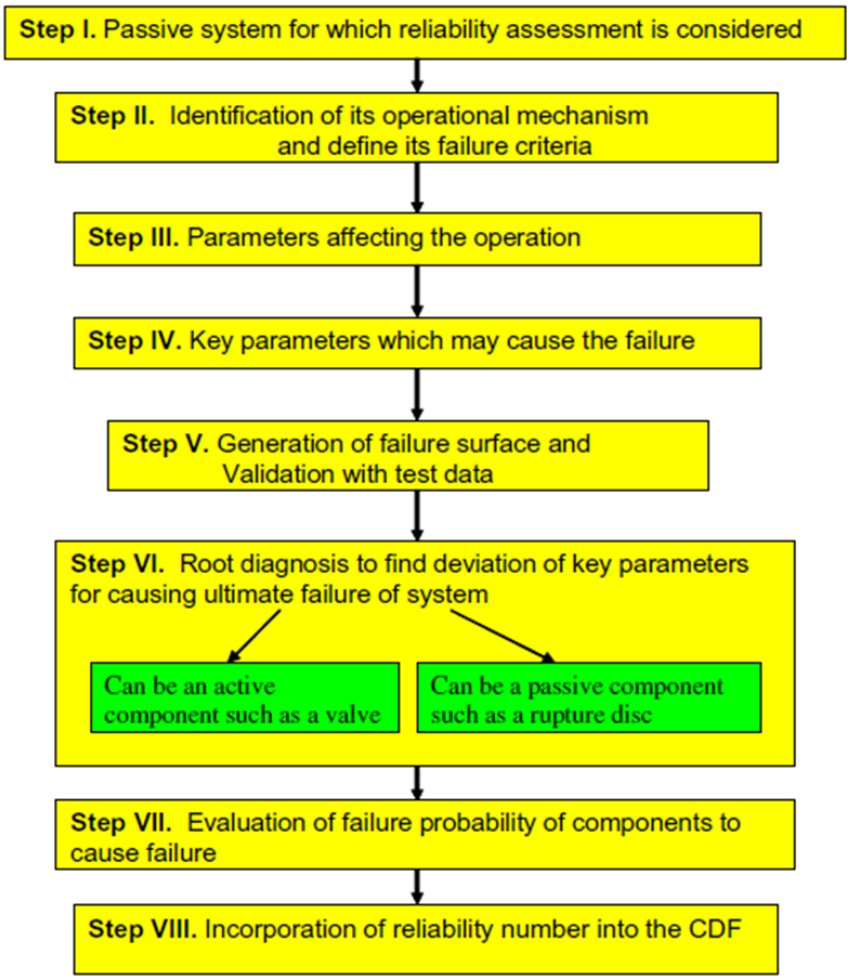

Figure 26: The workflow of ASPRA [62].

4.3.4. **ROAAM+**: Risk-Oriented Accident Analysis Methodology

ROAAM+ is a comprehensive framework designed to support decision-making under uncertainty in the evaluation of complex safety-critical systems [63, 64, 65, 66]. This method integrates deterministic and probabilistic analyses to address both aleatory uncertainties, which arise from inherent randomness in system behavior, and epistemic uncertainties, which are due to limited knowledge or incomplete data. Its applicability is especially significant in assessing rare, high-consequent scenarios (e.g. severe accidents, PSS failures) where traditional safety analysis methods (standalone DSA or PSA) are insufficient.

The primary purpose of ROAAM+ is to support robust risk-informed decision-making. This includes determining whether a system's reliability is acceptable, identifying dominant sources of uncertainty, and suggesting possible system modifications or improvements. It also enables integration with PSA, extending its capabilities by explicitly modeling phenomenological failure mechanisms and their interactions under various scenarios. Unlike conventional methods that may rely on best-estimate values or expert judgment alone, ROAAM+ provides a structured means to quantify the probability of failure, assess the impact of modeling assumptions, and delineate the boundary between success and failure through rigorous treatment of uncertainties.

The conceptual foundation of ROAAM+ lies in representing risk as a joint Probability Density Function (PDF), of frequency $\boldsymbol{f_i}$ and probability $\boldsymbol{P_i}$ of consequences $\boldsymbol{c_i}$ associated with a scenario $\boldsymbol{s_i}$, i.e. $\{\boldsymbol{s_i}, \boldsymbol{pdf}(\boldsymbol{f_i}, \boldsymbol{P_i}(\boldsymbol{c_i}))\}$. The methodology distinctly separates aleatory and epistemic uncertainties and employs advanced sampling strategies, such as second-order Monte Carlo simulations and adaptive sampling refinement, to efficiently explore the parameter space. In cases where parameter distributions are unknown or incomplete, the method provides tools such as splintering and second-order uncertainty quantification to capture the intangible aspects of the analysis.

Sensitivity, uncertainty, and risk analyses are conducted using the top layer of the ROAAM+ framework. This layer is designed to enable efficient exploration of complex system behavior by decomposing the accident progression into a set of causal relationships (CRs). Each CR encapsulates a distinct physical or phenomenological process contributing to system failure. The entire workflow of ROAAM+ treatment for each individual process is illustrated in Figure 27.

FOMs, typically associated with system loads or capacities, are formulated to represent risk-relevant outcomes. The analysis proceeds with the development of high-fidelity Full Models (FMs) using state-of-the-art simulation tools such as System Thermal-Hydraulic (STH) or Computational Fluid Dynamics (CFD) codes. These models are used to generate a database of transient solutions that reflect a wide spectrum of possible system behaviors under different conditions. To manage computational intensity and enable large-scale sampling, Surrogate Models (SMs) are constructed using data-driven techniques. These models are trained and validated against FM outputs. This modular representation facilitates systematic propagation of uncertainties, allowing for detailed sensitivity analysis, identification of dominant failure contributors.

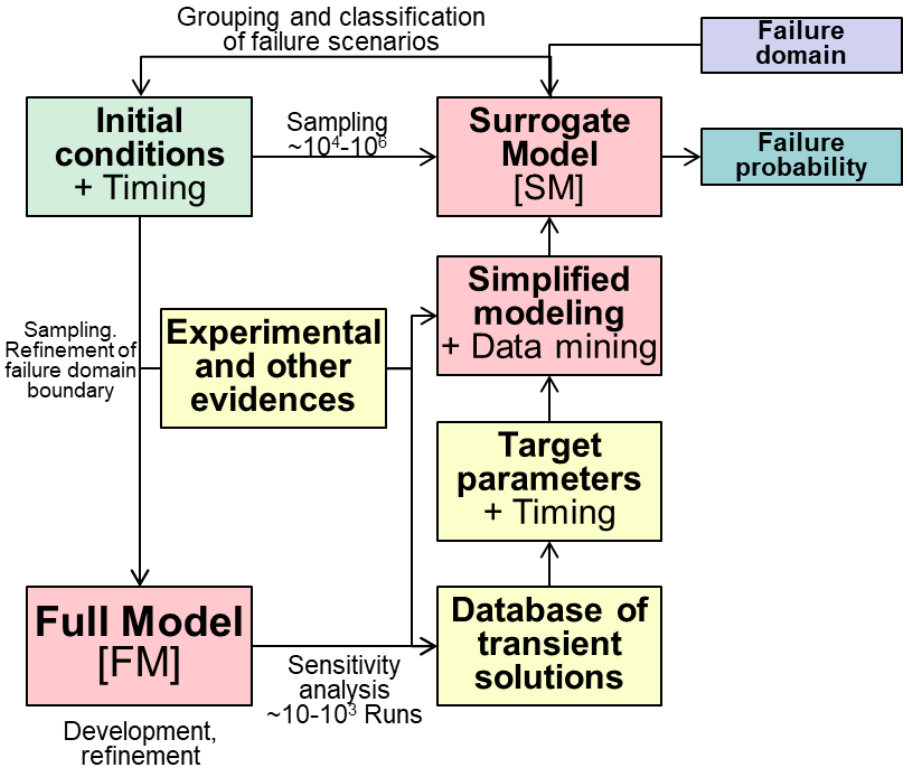

Figure 27: ROAAM+ workflow chart for a distinct physical or phenomenological process [63].

An advantage of ROAAM+ framework is its aim to reduce the user-effects in the reliability assessment. All introduced assumptions, approximations, and simplifications are explicitly recorded and their influence on the analysis outcomes is quantitatively assessed. This level of traceability ensures full transparency, facilitating thorough peer or regulatory review and strengthening the credibility and defensibility of the final safety-related decisions.

ROAAM+ is inherently adaptive. If expert reviews find a previously unaccounted-for phenomenon, the framework enables a conservative estimation of its potential impact on the modeling uncertainty and the resulting decision. Should the inclusion of this phenomenon have no effect on the outcome, no further action is necessary. Conversely, if the phenomenon could alter the decision, the relevant models must be updated to incorporate the new element, and the ROAAM+ process is re-applied in a new iteration.

The complexity of developing SM and defining appropriate FOMs within ROAAM+ depends on several factors, including the complexity of the physical models, the dimensionality of the input parameter space, and the characteristics of the failure domains. In cases with limited input variables and well-behaved phenomena, development of SM can be relatively straightforward. However, when causal relationships involve strong nonlinearities, mutual feedback mechanisms, or high-dimensional uncertainty spaces, constructing accurate and representative SM becomes significantly more demanding in terms of both computational effort and methodological robustness.

4.4. Knowledge gaps and challenges

Among methods introduced in Section 4.3, a key challenge in the reliability analysis of PSS is the accurate and efficient identification of failure domain (FD) regions in the input space where the system fails to meet performance criteria. This task is inherently difficult due to the complex, nonlinear, and time-dependent nature of the physical processes that govern passive system behavior.

Accurate failure domain identification typically requires the use of STH simulation tools (e.g. RELAP5, GOTHIC, MELCOR). These simulations, referred to as FMs, can capture the complex transient responses of the system under various input conditions. However, each individual simulation may require several hours or days to complete. When the input space is high-dimensional, meaning a large number of uncertain parameters must be considered simultaneously, a comprehensive exploration of all possible input combinations becomes computationally prohibitive. As dimensionality increases, the total number of simulations needed for reliable domain mapping grows exponentially, making brute-force methods infeasible.

To reduce computational burden, researchers often employ SMs as an approximation of the full model. These SMs are trained using a limited set of full model simulations and can then be used to rapidly evaluate system performance across the input space. This approach significantly reduces the time required to identify potential failure conditions. However, surrogate modeling introduces new limitations. The accuracy of the SMs depends heavily on the quality and representativeness of the training data. In particular, there is a risk that the SMs may fail to capture narrow or irregularly shaped failure regions that are poorly sampled during training. As a result, some true failure conditions may be misclassified as successful, which compromises the reliability assessment.

An alternative approach is to retain the FMs and improve the efficiency of the sampling strategy used to explore the input space. Adaptive algorithms such as genetic algorithms can be employed to improve sampling efforts near the estimated boundary between successful and failed conditions. These methods seek to extract the maximum amount of information from each simulation by guiding the search toward regions of high uncertainty or potential failure. Although this approach preserves the fidelity of the full model, it presents its own challenges. Designing an adaptive strategy that ensures sufficient global coverage of the input space, avoids convergence to local optima, and remains computationally tractable is a nontrivial task. Additionally, the stochastic nature of many search algorithms can lead to variability in the final identified failure domain, raising concerns about consistency and reproducibility.

ACKNOWLEDGEMENTS

Financial support from the SSM and Nordic Nuclear Safety Program (NKS) is greatly acknowledged. The authors are grateful to all the countries participating in the EU EASI-SMR project.

NKS conveys its gratitude to all organizations and persons who by means of financial support or contributions in kind have made the work presented in this report possible.

DISCLAIMER

The views expressed in this document remain the responsibility of the author(s) and do not necessarily reflect those of NKS. In particular, neither NKS nor any other organization or body supporting NKS activities can be held responsible for the material presented in this report.

REFERENCES

1. Li, H., Kudinov, P., 2010. Effective Approaches to Simulation of Thermal Stratification and Mixing in a Pressure Suppression Pool. OECD/NEA & IAEA Workshop CFD4NRS-3, Bethesda, MD, USA, September 14-16, 2010.
2. Li, H., Villanueva, W., Kudinov, P., 2014. Approach and Development of Effective Models for Simulation of Thermal Stratification and Mixing Induced by Steam Injection into a Large Pool of Water. Science and Technology of Nuclear Installations, 2014, Article ID 108782, 11 pages.
3. J. Laine, M. Puustinen, A. Räsänen, PPOOLEX Experiments with a Sparger, Nordic Nuclear Safety Research, 2015, NKS-334.
4. Mizokami, S., Yamada, D., Honda, T., Yamauchi, D., Yamanaka, Y., 2016. Unsolved issues related to thermal-hydraulics in the suppression chamber during Fukushima Daiichi accident progressions. Journal of Nuclear Science and Technology, 53, 630-638.
5. Mizokami, S., Yamanaka, Y., Watanabe, M., Honda, T., Fuji, T., Kojima, Y., PAIK, C.Y., Rahn, F., 2013. State of the art MAAP analysis and future improvements on TEPCO Fukushima-Daiichi NPP accident. NURETH-15: The 15th International Topical Meeting on Nuclear Reactor Thermal Hydraulics, Pisa, Italy, May 12-17, paper number 536.
6. Tanskanen, V., Jordan, A., Puustinen, M., Kyrki-Rajamäki, R., 2014. CFD simulation and pattern recognition analysis of the chugging condensation regime. Annals of Nuclear Energy, 66, 133-143.
7. Patel, G., Tanskanen, V., Hujala, E., Hyvärinen, J., 2017. Direct contact condensation modeling in pressure suppression pool system. Nuclear Engineering and Design, 321, 328-342.
8. Pellegrini, M., Naitoh, M., 2016. Application of two-phase flow DFC to the phenomena expected in Fukushima Daiichi S/C. OECD/NEA & IAEA Workshop CFD4NRS-6.
9. Li, H., Villanueva, W., Puustinen, M., Laine, J., Kudinov, P., 2014. Validation of Effective Models for Simulation of Thermal Stratification and Mixing Induced by Steam Injection into a Large Pool of Water. Science and Technology of Nuclear Installations, 2014, Article ID 752597, 18 pages.
10. Li, H., Villanueva, W., Puustinen, M., Laine, J., Kudinov, P., 2017. Thermal stratification and mixing in a suppression pool induced by direct steam injection. Annals of Nuclear Energy, 111, 487-498.
11. Villanueva, W., Li, H., Puustinen, M., Kudinov, P., 2015. Generalization of experimental data on amplitude and frequency of oscillations induced by steam injection into a subcooled pool. Nuclear Engineering and Design, 295, 155-161.
12. Li, H., Villanueva, W., Kudinov, P., 2011. Development and implementation of effective models in GOTHIC for the prediction of mixing and thermal stratification in a BWR pressure suppression pool. Proceedings of ICAPP 2011, Nice, France, May 2-5, 2011, Paper 11256.
13. Li, H. and Kudinov, P., 2008. An approach toward simulation and analysis of thermal stratification and mixing in a pressure suppression pool. NUTHOS-7, Seoul, Korea, October 5-9, Paper 243.
14. Gallego-Marcos, I., Villanueva, W., Kudinov, P., 2018. Modelling of Pool Stratification and Mixing Induced by Steam Injection through Blowdown Pipes. Annals of Nuclear Energy, 112, 624-639.
15. Li, H. and Kudinov, P., 2009. Condensation, Stratification and Mixing in a Boling Water Reactor Suppression Pool. NORTHNET Roadmap 3 Report, Division of Nuclear Power Safety, Royal Institute of Technology (KTH), Stockholm, Sweden, 70p.

16. Li, H., Villanueva, W., Kudinov, P., 2010. Investigation of containment behavior with activation of rupture disks in system 361/362 with GOTHIC simulation. Swedish Radiation Safety Authority (SSM) Project Report, Royal Institute of Technology (KTH), Stockholm, Sweden, 25p.
17. Li, H., Kudinov, P., Villanueva, W., 2010. Modeling of Condensation, Stratification and Mixing Phenomena in a Pool of Water. NKS Report, NKS-225, Division of Nuclear Power Safety, KTH, Stockholm, Sweden, 91p.
18. Li, H., Kudinov, P., Villanueva, W., 2010. Condensation, Stratification and Mixing in a Boling Water Reactor Suppression Pool. NORTHNET Roadmap 3 Report, Division of Nuclear Power Safety, Royal Institute of Technology (KTH), Stockholm, Sweden, 88p.
19. Li, H., Villanueva, W., Kudinov, P., 2012. Development, Implementation and Validation of EHS/EMS Models for Spargers. Westinghouse project report. Division of Nuclear Power Safety, Royal Institute of Technology (KTH), Stockholm, Sweden, 98p.
20. Li, H., Villanueva, W., Kudinov, P., 2012. Effective Momentum and Heat Flux Models for Simulation of Stratification and Mixing in a Large Pool of Water. NKS-ENPOOL Research report, NKS-266, 58p.
21. Li, H., Villanueva, W., Kudinov, P., 2012 Effective Models for Prediction of Stratification and Mixing Phenomena in a BWR Suppression Pool. NORTHNET Roadmap 3 Report, Division of Nuclear Power Safety, Royal Institute of Technology (KTH), Stockholm, Sweden, 87p.
22. Li, H., Villanueva, W., Kudinov, P., 2014. Effective Models for Simulation of Thermal Stratification and Mixing Induced by Steam Injection into a Large Pool of Water. Nordic Nuclear Safety Research, NKS-316.
23. Gallego-Marcos, I., Villanueva, W., Kapulla, R., Paranjape. S., Paladino, D., Kudinov, K., 2016. Modeling of thermal stratification and mixing induced by steam injection through spargers into a large water pool. OECD/NEA & IAEA Workshop CFD4NRS-6, Cambridge, MA, USA, September 13-15.
24. Gallego-Marcos, I., Villanueva, W., Kapulla, R., Paranjape. S., Paladino, D., Kudinov, K., 2016. Scaling and CFD Modelling of the Pool Experiments with Spargers Performed in the PANDA Facility. NUTHOS-11: The 11th International Topical Meeting on Nuclear Reactor Thermal Hydraulics, Operation and Safety Gyeongju, Korea, October 9-13, N11P0670.
25. Gallego-Marcos, I., Villanueva, W., Kudinov, P., 2016. Scaling of the Erosion of a Thermally Stratified Layer in a Large Water Pool during a Steam Injection Through Spargers. NUTHOS-11: The 11th International Topical Meeting on Nuclear Reactor Thermal Hydraulics, Operation and Safety, Gyeongju, Korea, October 9-13, N11P0525.
26. Gallego-Marcos, I., Villanueva, W., Kudinov, P., 2016. Modeling of Thermal Stratification and Mixing in a Pressure Suppression Pool Using GOTHIC. NUTHOS-11: The 11th International Topical Meeting on Nuclear Reactor Thermal Hydraulics, Operation and Safety, Gyeongju, Korea, October 9-13, N11P0524.
27. Gallego-Marcos, I., Kudinov, P., Villanueva, W., Kapulla, R., Paranjape, S., Paladino, D., Laine, J., Puustinen, M, Räsänen, A., Pyy, L., Kotro, E., 2019. Pool Stratification and Mixing Induced by Steam Injection through Spargers: CFD modeling of the PPOOLEX and PANDA experiments. Nuclear Engineering and Design, 347, 67-85.
28. Gallego-Marcos, I., Filich, L., Villanueva, W., Kudinov, P., 2015. Modelling of the Effects of Steam Injection through Spargers on Pool Thermal Stratification and Mixing. NKS Report 347.
29. Gallego-Marcos, I. Villanueva, W., Kudinov, P., 2016. Thermal Stratification and Mixing in a Large Pool Induced by Operation of Spargers, Nozzles, and Blowdown Pipes". NKS Report 369.

30. Gallego-Marcos, I., Villanueva, W., Kudinov, P., 2017. Modelling of a Large Water Pool during Operation of Blowdown Pipes, Spargers, and Nozzles. NKS-393.
31. Puustinen, M., Laine, J., Räsänen, A., 2009. PPOOLEX experiments on thermal stratification and mixing. Research report CONDEX 1/2008, NKS-198.
32. Gallego-Marcos I., Kudinov P., Villanueva W., Kapulla R., Paranjape S., Paladino D., Laine J., Puustinen M., Räsänen A., Pyy L., Kotro E., 2018. Pool Stratification and Mixing Induced by Steam Injection through Spargers: analysis of the PPOOLEX and PANDA experiments. Nuclear Engineering and Design, 337, 300-316.
33. M. Puustinen, J. Laine., 2011. A. Räsänen, Multiple blowdown pipe experiments with the PPOOLEX facility, Nordic Nuclear Safety Research NKS-241.
34. Gallego-Marcos, I., Grishchenko, D., Kudinov, P., 2019. Thermal stratification and mixing in a Nordic BWR pressure suppression pool. Annals of Nuclear Energy, 132, 442-450.
35. Gallego-Marcos, I. Kudinov P., Villanueva W., Puustinen M, Räsänen A., Tielinen K., Kotro E., 2019. Effective momentum induced by steam condensation in the oscillatory bubble regime. Nuclear Engineering and Design, 350, 259-274.
36. GOTHIC Thermal Hydraulic Analysis Package, Version 8.1(QA). EPRI, Palo Alto, CA: 2014.
37. RELAP5/MOD3.3 Code Manual Volume IV. US Nuclear Regulatory Commission, Washington DC, 2006.
38. Paladino, D., Dreier, J., 2012. PANDA: a multipurpose integral test facility for LWR safety investigations. Science and Technology of Nuclear Installations, Article ID 239319.
39. ANSYS® Academic Research, 2021 R2, ANSYS Fluent Theory Guide, ANSYS, Inc.
40. Kudinov, P., Wang, X., Grishchenko, D., Puustinen, M., Räsänen, A., Kotro, E., Tielinen, K., Pättikangas, T., Silde, A. 2020. Thermal Hydraulic Phenomena of the Suppression Pool. NKS-THEOS Report, NKS-439.
41. Wang, X., Grishchenko, D, Kudinov, P. 2020. Development of Effective Momentum Model for Steam Injection Through Multi-Hole Spargers Using a Condensation Region Approach. *ICONE-2020*. Virtual, Online. August 4–5, V001T03A025. ASME.
42. Wang, X., Grishchenko, D, Kudinov, P. 2021. Development of Effective Momentum Model for Steam Injection Through Multi-Hole Spargers: Unit Cell Model. *ICONE-28*. Virtual, Online. August 4–6
43. Wang, X., Grishchenko, D., Kudinov, P. "Pre-test analysis for definition of steam injection tests through multi-hole sparger in PANDA facility", *Nucl. Eng. Des*, *386*, 111573 (2021).
44. Wang, X., Grishchenko, D., Kudinov, P. Simulation of jets induced by steam injection through multi-hole sparger using effective heat and momentum models. Nuclear Engineering and Design, 405 112222. (2023).
45. Wang, X., Kudinov, P., Grishchenko, D., et al. Momentum source induced by steam injection into a subcooled pool, International journal of heat and mass transfer, 232, 125969, (2024).
46. Wang, X., Acharya, G., Grishchenko, D., Kudinov, P. CFD simulation of thermal stratification and mixing in a Nordic pressure suppression pool, Nuclear Engineering and Technology. 56(12), 5357-5376, (2024).
47. Wang, X. Thermal stratification and mixing induced by steam injection into a pressure suppression pool, (PhD dissertation). https://urn.kb.se/resolve?urn=urn:nbn:se:kth:diva-360120, 2025.

48. M. Jeltsov., D. Grishchenko., P. Kudinov. “Validation of Star-CCM+ for liquid metal thermal-hydraulics using TALL-3D experiment”, Nuclear Engineering and Design, 341, 306-325, (2019).
49. R. Everson and L. Sirovich, “Karhunen–loéve procedure for gappy data”, J. Opt. Soc. Amer. A, Opt. Image Sci., vol. 12, no. 8, pp. 1657–1664, (1995).
50. K. Manohar, B. W. Brunton, J. N. Kutz, and S. L. Brunton, “Data-driven sparse sensor placement for reconstruction: Demonstrating the benefits of exploiting known patterns,” IEEE Control Syst. Mag., 38(3), 63–86, (2018).
51. Program on Technology Innovation: Comprehensive Risk Assessment Requirements for Passive Safety Systems. EPRI, Palo Alto, CA; 2008. 1016747.
52. A. K. Nayak., A. Chandrakar., and G. Vinod. “A review: Passive system reliability analysis – accomplishments and unresolved issues”, Frontiers in Energy Research, vol 2, (2014).
53. F. Bianchi, L. Burgazzi, F. D’Auria, and M. E. Ricotti, “The REPAS approach to the evaluation of passive safety systems reliability,” NEA/CSNI/R(2002)10, pp. 133, (2002).
54. J. Jafari, F. D’Auria, H. Kazeminejad, and H. Davilu, “Reliability evaluation of a natural circulation system,” Nuclear Engineering and Design, 224(1), 79–104, (2003).
55. F. Pierro, D. Araneo, G. Galassi, and F. D’Auria, “Application of REPAS methodology to assess the reliability of passive safety systems,” Science and Technology of Nuclear Installations, 2009(1), Article ID 768947, (2009).
56. A. Bersano, G. Grippo, G. Agnello, E. Zio, and F. Mascari, “Application of REPAS to analyze the sump clogging issue following a LOCA and its impact on the reliability of the ECCS long-term core cooling function,” Nuclear Engineering and Design, 417, 112877, (2024).
57. S. S. Wilks, “Determination of sample sizes for setting tolerance limits,” Annals of Mathematical Statistics, 12(1), 91–96, (1941).
58. S. S. Wilks, “Statistical prediction with special reference to the problem of tolerance limits,” Annals of Mathematical Statistics, 13(4), 400–409, (1942).
59. M. Marques, J. F. Pignatel, P. Saignes, L. D’Auria, C. Muller, C. Bolado-Lavin, C. Kirchsteiger, V. La Lumina, and L. Ivanov, “Methodology for the reliability evaluation of a passive system and its integration into a probabilistic safety assessment,” Nuclear Engineering and Design, 235, 2612–2631, (2005).
60. Progress in Methodologies for the Assessment of Passive Safety System Reliability in Advanced Reactors - IAEA TECDOC TE-1752 RMPS (2014).
61. A.K. Nayak, M.R. Gartia, A. Antony, G. Vinod and R.K. Sinha, Reliability Analysis of a Boiling Two-phase Natural Circulation System Using the APSRA Methodology, Proceedings of ICAPP 2007, Nice, France, May 13-18, 2007.
62. A. K. Nayak, M. R. Gartia, A. Antony, G. Vinod, and R. K. Sinha, “Passive system reliability analysis using APSRA methodology,” Nuclear Engineering and Design, (2008).
63. P. Kudinov, S. Galushin, D. Grishchenko, and S. Yakush, “Development of risk-oriented accident analysis methodology (ROAAM+) for assessment of ex-vessel severe accident management effectiveness,” *Proceedings of NURETH-18*, 2519–2535, (2019).
64. Galushin, S., Grishchenko, D., Kudinov, P. “Implementation of framework for assessment of severe accident management effectiveness in Nordic BWR,” Reliability Engineering and System Safety, 203, art. no. 107049 (2020)
65. Galushin, S., Grishchenko, D., and Kudinov, P. “Analysis of the Effect of Vessel Failure and Melt Release on Risk of Containment Failure Due to Ex-Vessel Steam Explosion in Nordic Boiling Water Reactor Using ROAAM+ Framework.”. ASME J of Nuclear Rad Sci. October 2020; 6(4): 041113. https://doi.org/10.1115/1.4047552, 2020.

66. Grishchenko D., Galushin S., Kudinov P., “Failure domain analysis and uncertainty quantification using surrogate models for steam explosion in a Nordic type BWR”, Nuclear Engineering and Design, Volume 343, 2019, Pages 63-75, ISSN 0029-5493, 2019.

Bibliographic Data Sheet **NKS-502**

Title	Passive safety system performance of SMRs
Author(s)	Xicheng Wang[1], Dmitry Grishchenko[1], Pavel Kudinov[1]
Affiliation(s)	[1]Division of Nuclear Science and Engineering, Royal Institute of Technology (KTH).
ISBN	978-87-7893-600-4
Date	June 2025
Project	NKS-R / PAS-SMR
No. of pages	49
No. of tables	4
No. of illustrations	27
No. of references	66
Abstract max. 2000 characters	This work aims to develop and validate modeling approaches for key Passive Safety System (PSS) phenomena, and to establish reliability assessment methodologies. A major focus is steam condensation in water pools, commonly used as SMR heat sinks, where temperature distribution strongly influences natural circulation and passive heat removal. Due to limited predictive capabilities, the development of mechanistic model and large-scale experiments have been initiated, including several international projects. This report details analytical support for the OECD/NEA PANDA tests on steam injection into a water pool. Five tests were designed to address uncertainties in thermal stratification and mixing under pressurized, near-saturation conditions, using data-driven sensor placement for thermocouple positioning and combined Particle Image Velocimetry (PIV) to capture velocity and temperature profiles. The report also reviews recent advances in PSS reliability analysis, emphasizing challenges in efficiently identifying Failure Domains (FDs).
Key words	Steam Condensation, Pool Stratification, Passive Safety System, Reliability Analysis, Small Modular Reactors.

Available on request from the NKS Secretariat, P.O.Box 49, DK-4000 Roskilde, Denmark.
Phone (+45) 4677 4041, e-mail nks@nks.org, www.nks.org